# The ultimate arc: Differential displacement, oroclinal bending, and vertical axis rotation in the External Betic-Rif arc

J. P. Platt,[1] S. Allerton,[2] A. Kirker,[2] C. Mandeville,[2] A. Mayfield,[1] E. S. Platzman,[1] and A. Rimi[3]

Received 20 August 2001; revised 27 August 2002; accepted 16 September 2002; published 9 May 2003.

[1] The External Betic-Rif arc, which lies between the converging African and Iberian plates, is one of the tightest orogenic arcs on Earth. It is a thin-skinned fold and thrust belt formed in Miocene time around the periphery of the Alborán Domain, an older contractional orogen that underwent extensional collapse coevally with the formation of the thrust belt. Restoration of four sections across the thrust belt, together with kinematic and paleomagnetic analysis, allows a reconstruction of the prethrusting geometry of the Alborán Domain, and the identification of the following processes that contributed to the formation of the arc: (1) The Alborán Domain moved some 250 km westward relative to Iberia and Africa during the Miocene. This initiated the two limbs of the arc on its NW and SW margins, closing to the WSW in the region of Cherafat in northern Morocco. The overall convergence direction on the Iberian side of the arc was between 310° and 295°, and on the African side it was between 235° and 215°. The difference in convergence direction between the two sectors was primarily a result of the relative motion between Africa and Iberia. (2) Extensional collapse of the Alborán Domain during the Miocene modified the geometry of the western end of the arc: the Internal Rif rotated anticlockwise to form the present north trending sector of the arc, and additional components of displacement produced by extension were transferred into the external thrust belt along a series of strike-slip faults and shear zones. These allowed the limbs of the arc to rotate and extend, tightening the arc, and creating variations in the amounts and directions of shortening around the arc. The Betic sector of the arc rotated clockwise by 25° during this process, and the southern Rif rotated anticlockwise by ~55°. (3) Oblique convergence on the two limbs of the arc, dextral in the Betics and sinistral in the southern Rif, resulted in strongly noncoaxial deformation. This had three related effects: (1) large rotations of individual thrust sheets resulted from the oblique propagation of thrusts away from the thrust front, followed by pinning and rotation as the thrust sheets peeled off, (2) continued oblique convergence resulted in distributed shear, particularly in the rear of the thrust wedge, causing rotation of stacks of thrust sheets on the scale of a few tens of kilometers, and (3) distributed shear in the orogen resulted in the rotation of folds as they amplified, the hinges migrating through the rock body, and rotating at a slower rate than the rock. These rotations were substantially larger than the bulk rotations of the limbs of the arc, and they strongly modified the orientations of folds, thrust traces, and the structural indicators of fault slip directions. *INDEX TERMS:* 8102 Tectonophysics: Continental contractional orogenic belts; 8150 Tectonophysics: Evolution of the Earth: Plate boundary—general (3040); 1525 Geomagnetism and Paleomagnetism: Paleomagnetism applied to tectonics (regional, global); 8010 Structural Geology: Fractures and faults; 8005 Structural Geology: Folds and folding; *KEYWORDS:* paleomagnetism, thrust, orocline, Spain, Mediterranean, arc. **Citation:** Platt, J. P., S. Allerton, A. Kirker, C. Mandeville, A. Mayfield, E. S. Platzman, and A. Rimi, The ultimate arc: Differential displacement, oroclinal bending, and vertical axis rotation in the External Betic-Rif arc, *Tectonics*, *22*(3), 1017, doi:10.1029/2001TC001321, 2003.

## 1. Introduction

[2] Geologists have been puzzled by the highly arcuate nature of many compressional mountain chains since at least the time of *Argand* [1924], who documented the sinuous character of the whole Alpine-Himalayan system, from Gibraltar to SE Asia. Several fundamental questions are posed by these structures. (1) Is the arcuate geometry primary, or was it developed or accentuated during or after compressional tectonics within the mountain chain [*Carey*, 1955; *Marshak*, 1988; *Hindle and Burkhard*, 1999]? (2) Do the directions and amounts of shortening and thrust transport remain constant around the arc, or do they vary? (3) To what extent do arc-parallel extension and vertical axis rotation contribute to the development of the arc? (4) How are changes in the geometry of the arc accommodated in the forearc and back arc regions? (5) Can the geometrical evolution and the pattern of shortening directions be explained in terms of the motions of rigid plates bounded by the arcuate belt?

[1]Department of Earth Sciences, University College London, London, UK.
[2]Department of Earth Sciences, University of Oxford, Oxford, UK.
[3]Institut Scientifique, Université Mohammed V, Rabat, Morocco.

Copyright 2003 by the American Geophysical Union.
0278-7407/03/2001TC001321

[3] The aim of this paper is to address these questions through detailed structural and paleomagnetic analysis of the External Betic-Rif arc (Figures 1 and 2). The arc straddles the Africa-Eurasia plate boundary, but its geometry bears no obvious relationship to the history of relative motion between these two plates. It is defined by a thrust belt of Neogene age that surrounds the Alborán Sea, which is an extensional basin that developed more or less coevally with the thrust belt. Its youth, good subaerial exposure, striking geometry, and the well-defined plate boundary conditions during its formation make it an outstanding region for such a study.

[4] It is likely that arcuate geometry can be formed in more than one way and that the answers to the questions posed above are not the same for all arcs. Many of the volcanic island arcs in the western Pacific surround actively extending marginal basins and have probably increased their curvature as the back arc basin has grown, and this may also be true of some of the arcuate mountain chains in the Mediterranean region, such as the Calabrian arc [*Dewey et al.*, 1989; *Malinverno and Ryan*, 1986]. Other arcuate mountain chains such as the Alps, which do not have actively extending back arcs, formed with roughly their present geometry as a result of indentation by irregular continental margins [*Schmid and Kissling*, 2000]. In intracontinental settings, synorogenic bending has been proposed and explained as a result of buttressing against basement highs in the Idaho-Wyoming overthrust belt [*Grubbs and Van der Voo*, 1976] and the Fleurieu arc in South Australia [*Marshak and Flöttman*, 1996]. Many arcuate thrust belts appear to have developed as a result of variations in thickness of the sediment fill in a deformed basin (the Pennsylvania salient of the Appalachians [*Gray and Stamatakos*, 1997] and the Nackara arc in South Australia [*Marshak and Flöttman*, 1996] are examples), and vertical axis rotations may be a result of shear along the margins of the salient rather than wholesale rotation [*Macedo and Marshak*, 1999]. In the Bolivian arc, differential shortening, small block rotations, and wholesale rotation of parts of the orogen, have all been invoked to explain the geometry and pattern of vertical axis rotations [*Isacks*, 1988; *Beck et al.*, 1994; *McFadden et al.*, 1995]. The Kingston orocline in the Appalachians has been explained by the intersection of two thrust belts of different ages [*Marshak and Tabor*, 1989], whereas a strong case has been made for essentially postorogenic (oroclinal) bending in the Cantabria-Asturias Arc [*Weil et al.*, 2000].

[5] The directions of relative motion within actively converging arcuate belts can be determined from the seismicity: they vary around the arc in nearly all cases, but in some arcs (e.g., the Aleutians) the convergence direction is nearly constant around significant changes in trend [*McCaffrey*, 1994], whereas in others, such as the Himalayas, it remains almost orthogonal to the arc all the way around [*Baranowski et al.*, 1984; *Molnar and Lyon-Caen*, 1989]. The large-scale kinematics of the Aleutian arc can be described fairly precisely in terms of rigid plate tectonics: variations in the convergence direction can be attributed to partitioning of deformation among thrusting, strike-parallel slip, and strike-parallel extension within the arc itself [*McCaffrey*, 1994; *Ave-Lallemant*, 1996], whereas the geometry and kinematics of the Himalayan arc are profoundly influenced by the distributed deformation within the Tibetan Plateau and adjacent regions farther north, and the thrust belt cannot be described as a boundary between rigid plates.

## 2. Geological and Geophysical Background

[6] The Africa-Eurasia plate boundary in the eastern Atlantic is defined by the Azores fracture zone, a dextral transform that becomes more compressional in character eastward [*Sartori et al.*, 1994]. From the Gorringe bank eastward to Gibraltar, recent plate motion has been slow NW directed oblique convergence [*DeMets et al.*, 1990]. Present-day seismicity between Africa and Iberia is generally weak and distributed over a zone several hundred kilometers wide [*Calvert et al.*, 2000]; the largest events occur along the north African littoral and indicate NW directed convergence accommodated mainly on dextral strike-slip faults and conjugate sinistral faults [*Morel and Meghraoui*, 1996].

[7] The crust beneath the Betic and Rif mountain belts is 25–39 km thick [*Banda et al.*, 1983]; it thins below the Alborán Sea to 12–20 km [*Torné et al.*, 2000] but remains continental in character, being made up of metamorphic rocks comparable to those in the adjacent internal Betic and Rif orogens [*Soto and Platt*, 1999], with a cover of Neogene sediments and volcanics [*Comas et al.*, 1999]. Eastward, the Alborán Sea passes into the young oceanic crust of the Balearic basin.

[8] The depth distribution of the seismicity and the velocity structure revealed by seismic tomography suggest a complicated and remarkable lithospheric structure beneath the region. Beneath the Alborán Sea the lithosphere is exceptionally thin (<60 km) and is underlain by aseismic, low-velocity asthenosphere, but a zone of seismicity dips steeply south from beneath the western Betics to ~150 km beneath the Alborán Sea [*Seber et al.*, 1996; *Calvert et al.*, 2000]. A more diffuse zone of intermediate depth seismicity underlies the Rif. Seismic tomography suggests that the seismicity corresponds roughly to the boundary between the hot asthenosphere beneath the Alborán Sea and a zone of colder mantle that extends eastward from the Gibraltar region beneath it [*Calvert et al.*, 2000]. A NE trending vertical body of cold mantle lies between 200 and 400 km [*Blanco and Spakman*, 1993; *Calvert et al.*, 2000], and another such body lies at 500–650 km depth, including the source area for several powerful deep earthquakes [*Grimison and Chen*, 1986]. These structures have variously been interpreted as a detached slab of subducted oceanic lithosphere [*Blanco and Spakman*, 1993], or the result of delamination or convective removal of lithospheric mantle [*Seber et al.*, 1996; *Calvert et al.*, 2000].

[9] At the surface, the Betic-Rif orogen consists of an external thin-skinned fold-and-thrust belt that defines the arc, surrounding an internal predominantly metamorphic

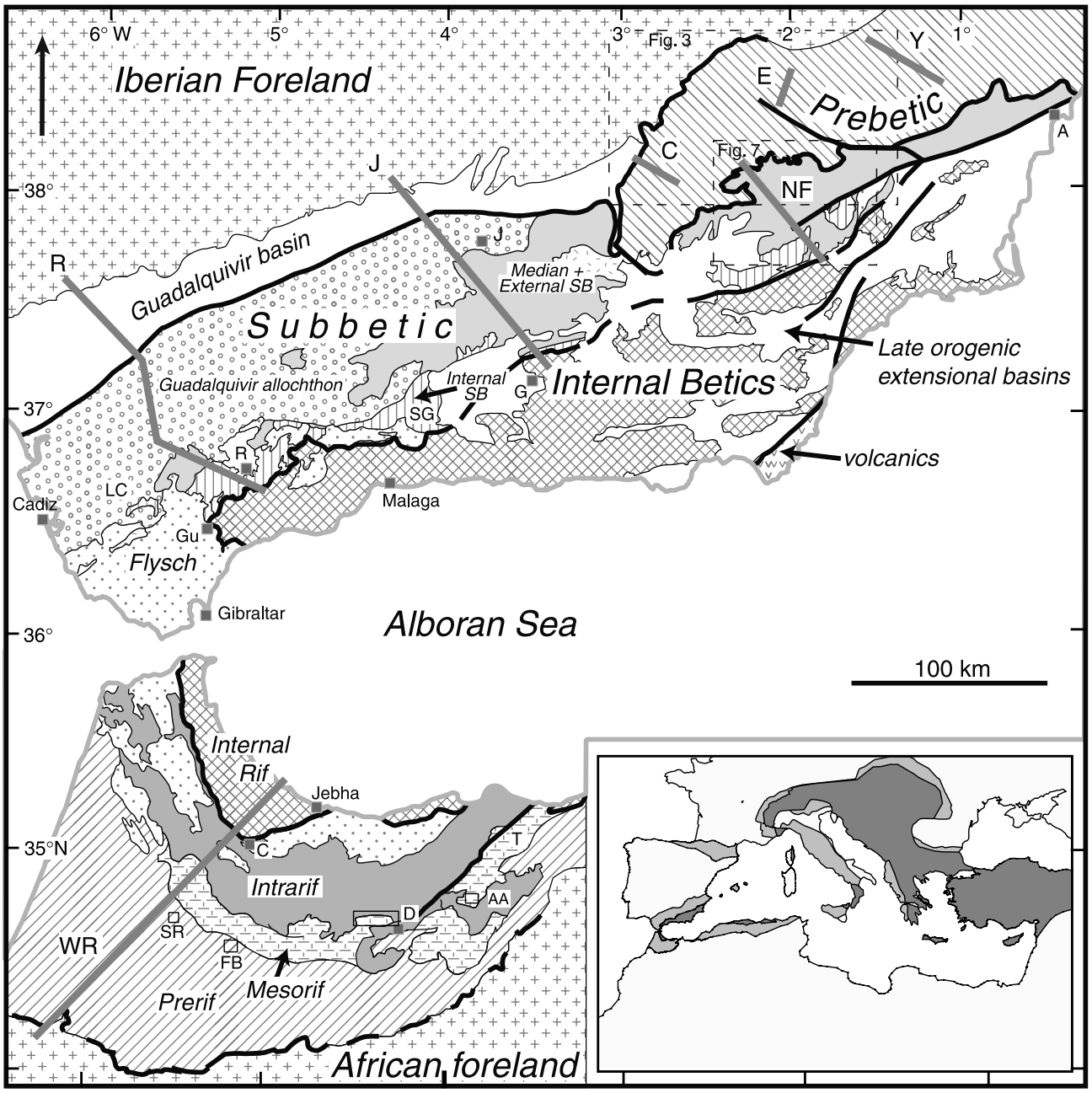


**Figure 1.** Tectonic map of Betic-Rif arc, after *Empreza Nacional Adara de Investigaciones Mineras S.A.* (ENADIMSA) [1985] and *Wildi* [1983]. External thrust belt comprises Prebetic and Subbetic Zones in Spain; Prerif, Mesorif, and Intrarif zones in Morocco; and Flysch nappes, which straddle the Straits of Gibraltar. Alborán Domain comprises Betic and Rif Internal Zones, together with floor of the Alborán Sea. A, Alicante; C, Cherafat; D, Dhar Souk; G, Granada; Gu, Gaucín; J, Jaén; LC, Las Cabras; R, Ronda; SG, Sierra Gorda; T, Temsamane massif. Restored sections indicated, from NE around arc, are Y, Yecla; E, Elche; C, Cazorla (Figure 5); NF, Nerpio-Fuensanta (Figure 8); J, Jaén (Figure 10); R, Ronda (Figure 11); and WR, Western Rif (Figure 14). Locations of Figures 2 and 3 and maps of Azrou Akchar (AA, Figure 16), Dhar Souk (D, Figure 18), Fes el Bali (FB, Figure 19), and Sidi Redouane (SR, Figure A of auxillary data) are shown. Inset shows position of Betic-Rif arc in context of Mediterranean Alpine chains. See color version of this figure at back of this issue.

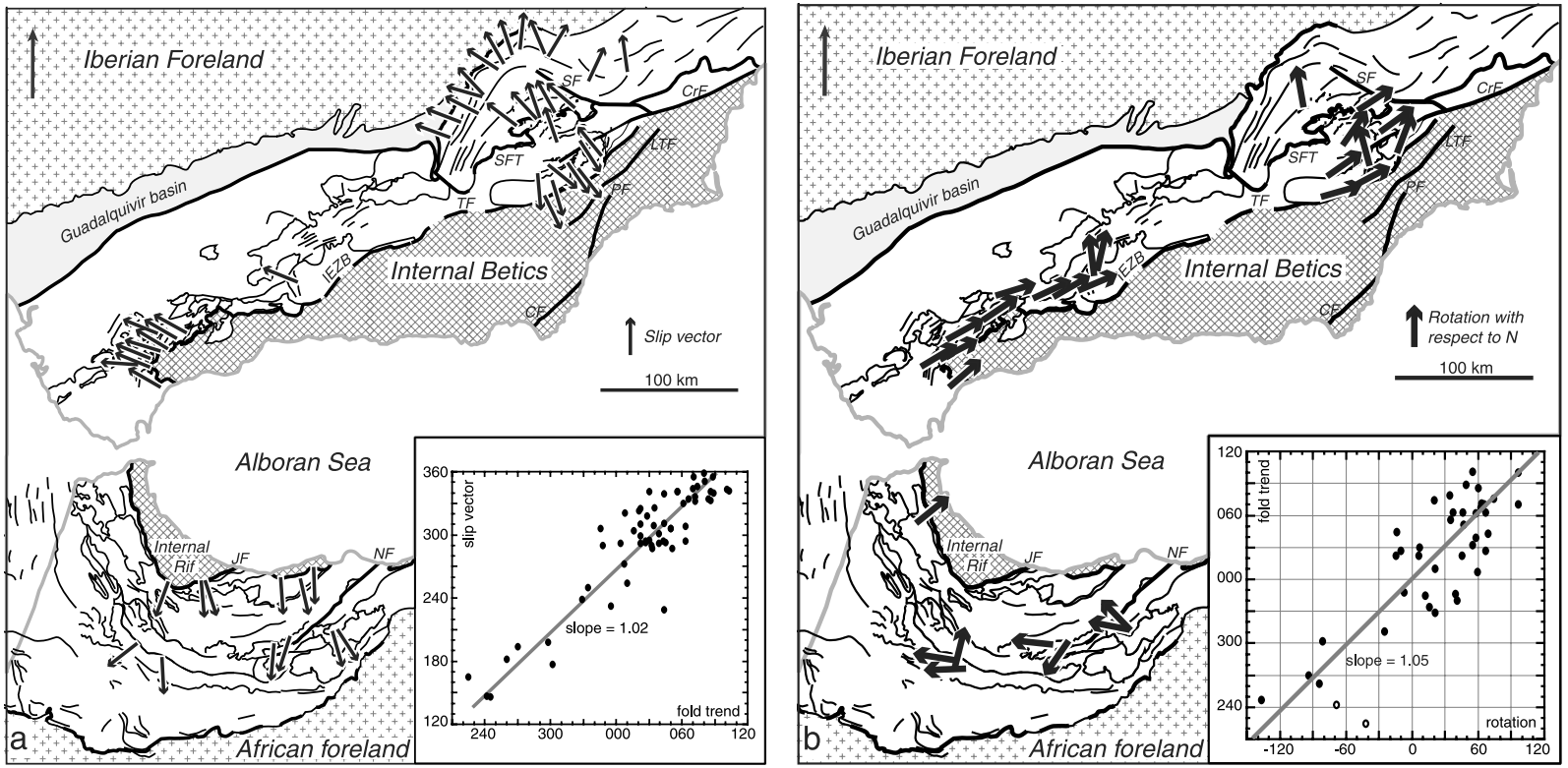


**Figure 2.** (a) Representative thrust-related slip vectors around External Betic-Rif arc. Head of arrow indicates sense of relative motion; foot of the arrow indicates location. Each arrow represents mean of several sites; 10–20 measurements were made at each site. Fold trends and thrust traces are shown in background. CF, Carboneras fault; CrF, Crevillente fault; IEZB, Internal External Zone Boundary; JF, Jebha Fault; LTF, Lorca Totana Fault; NF, Nekkor Fault; PF, Palomares Fault; SF, Socovos Fault; SFT, Subbetic Frontal Thrust; TF, Tiscar Fault. Inset shows correlation plot of slip vectors against structural trends around arc. (b) Representative vertical axis rotations around External Betic-Rif arc. Deviation of arrow from north indicates amount of vertical axis rotation with respect to reference direction for age of remanence and location of site within Iberian or African plate. Inset shows correlation plot of structural trends against vertical axis rotations around arc.

hinterland, known as the Alborán Domain, which comprises the Betic and Rif Internal Zones and the floor of the Alborán Sea. The external thrust belt swings from a WSW trend in the Betic Cordillera of southern Spain, through south across the Strait of Gibraltar into the northern Rif of Morocco, and round to east and ENE in the southern Rif. It is made up of a number of discrete geological elements that relay each other around the arc. These are (1) the Subbetic and Prebetic Zones of southern Spain, developed from the Mesozoic and Tertiary sediments that lay on the southern rifted margin of Iberia; (2) the so-called Flysch Units, comprising siliciclastic sediments of Cretaceous to early Miocene age, deposited in a deep marine or oceanic setting near the northern margin of Africa [*Didon et al.*, 1973], and (3) the External Rif, formed from Mesozoic and Tertiary sediments on the rifted African margin [*Wildi*, 1983; *Favre et al.*, 1991]. Although no geological unit can be traced all the way round the arc, there are no discrete or abrupt changes in the geology, the structural style, or the trend. The main phase of contractional deformation is coeval around the external arc, starting in Burdigalian (early Miocene) time on the inside of the arc and becoming progressively younger to Tortonian (late Miocene) near the outer margin.

[10] The Alborán Domain, which lies in the core of the arc, comprises the remains of a contractional mountain belt of probable Paleogene age. This region was affected by high-pressure low-temperature metamorphism [*Puga et al.*, 1999; *Azañón and Crespo-Blanc*, 2000], evolving to higher temperature and lower pressure during a pervasive extensional tectonic event of early Miocene age [*Platt et al.*, 1998; *Argles et al.*, 1999; *Platt and Whitehouse*, 1999] that created a suite of sedimentary basins, including the present-day Alborán Sea [*Watts et al.*, 1993]. The Alborán Domain lies in thrust contact with the External Zones along the Internal/External Zone Boundary (IEZB), and at least half the present-day crustal thickness beneath the Internal Zones consists of continental basement that originally underlay the sediments of the external thrust belt [*Watts et al.*, 1993; *Carbonell et al.*, 1998].

[11] At present, this zone of overall plate convergence is entirely intracontinental in character, and there is no unequivocal evidence that oceanic lithosphere was ever involved. A disrupted layer of mafic and ultramafic rocks in the Internal Betics has been interpreted as the remains of an ophiolite sequence [e.g., *Puga et al.*, 1999], but the primary relationships have been obscured by pre-Neogene deformation and metamorphism. Cretaceous sedimentation in the Median Subbetic and Flysch domains locally took place below carbonate compensation depth, but these rocks appear to overlie Triassic evaporites deposited in a continental setting.

[12] The large-scale plate tectonic history of the region involved sinistrally oblique extension in Triassic to mid-Cretaceous time, which opened up a narrow seaway connecting the Atlantic to the Neotethys ocean [*Dewey et al.*, 1989; *Roest and Srivastava*, 1992]. Convergence started in Late Cretaceous or Early Tertiary time, as Africa moved NE and then north with respect to Europe. The detailed plate motion history is complicated by the independent motion of Iberia since the Early Cretaceous [*Roest and Srivastava*, 1992]. During the Tertiary, Africa and Iberia converged in a roughly N-S to NW-SE direction by between 200 and 500 km, and they continue to do so today [*DeMets et al.*, 1990]. The plate tectonic setting therefore provides no obvious explanation for the arcuate geometry.

[13] A possible solution is to involve an additional plate, and *Andrieux et al.* [1971] postulated an Alborán microplate that moved westward between Africa and Iberia, producing the Gibraltar segment of the arc by frontal convergence. In this interpretation the ''limbs'' of the arc would be predominantly strike slip in character: dextral in the Betic Cordillera and sinistral in the Rif. Elaborations on this theme were developed by *Leblanc and Olivier* [1984] and *Sanz de Galdeano* [1990], and the importance of dextral strike-slip motion in the formation of the Betic Cordillera in particular was emphasized by *Hermes* [1978] and *De Smet* [1984].

[14] The microplate hypothesis fails, however, to explain the large-scale Neogene extension in the Alborán Domain [*Platt and Vissers*, 1989; *Comas et al.*, 1999; *Crespo-Blanc*, 1995; *Jabaloy et al.*, 1993; *Watts et al.*, 1993]. This has led to alternative hypotheses, involving either back arc extension behind a retreating subduction zone [*Lonergan and White*, 1997; *Royden*, 1993], extensional collapse of the earlier collisional orogen caused by convective removal of a thickened lithospheric root [*Platt and Vissers*, 1989; *Vissers et al.*, 1995], slab detachment [*Blanco and Spakman*, 1993], or delamination of lithospheric mantle [*Comas et al.*, 1992; *Platt et al.*, 1998]. These ideas have varying implications for the amount and direction of relative motion within the arcuate system, but surprisingly little information has been available on the kinematics of the external thrust belt. *Frizon de Lamotte* [1987] has presented evidence for SW directed sinistral shear in the Temsamane region of the southeastern external Rif, and *Guezou et al.* [1991] have argued for dominantly west directed thrusting within the system based on data from the western part of the Prebetic arc (Figure 1). *Lonergan et al.* [1994] present evidence for roughly NW-SE convergence along the IEZB in the eastern Subbetics, whereas in the west the direction was around WNW [*Platt et al.*,1995; *Kirker and Platt*, 1998].

## 3. Aims and Methods

### 3.1. Structural Data

[15] A primary purpose of this paper is to present a complete set of new and previously published data on the kinematics of the external thrust belt from right around the system (Table 1) and to discuss the implications of these data for the origin of the arc. The data consist of linear indicators such as striations, crystal fiber lineations, and solution grooves on fault planes that indicate the direction of fault slip, taken together with the orientation of gouge fabrics and Riedel fracture orientations relative to the fault slip plane as indicators of the sense of slip [e.g., *Petit*, 1987]. Measurements were made in fault zones related to clearly identifiable and mappable thrust surfaces. Between

**Table 1.** Summary of Slip Vector Azimuth, Structural Trend, and Rotation Data[a]

| Site | SV | Trend | *R* | Source |
|---|---|---|---|---|
| | | *Eastern Subbetics* | | |
| B49 Prebetic | | 027 ± 10 | −10 ± 6.4 | |
| Espuña | 304 ± 8 | 016 ± 10 | | LPG |
| Velez Rubio | 334 ± 10 | 066 ± 10 | | LPG |
| Velez Blanco | 359 ± 9 | 080 ± 10 | | TP |
| Ponce B401 | 321 ± 12 | 008 ± 10 | | TP |
| Mean Ponce | 254 ± 8.8 | 010 ± 10 | 21 ± 8 | TP |
| Mean Almirez | 325 ± 6.3 | 022 ± 10 | −15 ± 6 | TP |
| Luchena | 341 ± 9.8 | 030 ± 10 | | TP |
| Perugio | 323 ± 8.3 | 021 ± 10 | | TP |
| G2 | 355 ± 14.4 | 088 ± 10 | | TP |
| Cantar | 309 ± 9.7 | 034 ± 10 | | TP |
| Burete fold | 339 ± 18 | 044 ± 10 | −14 ± 15 | TP |
| Burete 2 | 229 ± 11 | 044 ± 10 | −14 ± 15 | TP |
| Mojantes | 341 ± 6.5 | 056 ± 10 | 35 ± 5 | TP |
| Quipar N | 358 ± 17 | | | TP |
| Quipar S | 327 ± 19 | | 54 ± 16.3 | TP |
| AA Almirez | 310 ± 8.9 | 022 ± 10 | 6 ± 13.4 | M |
| CA Alcaide | 340 ± 10 | 089 ± 10 | 49 ± 10.3 | M |
| CB Gabar | 355 ± 10 | 071 ± 10 | 63 ± 5.5 | M |
| CC | 344 ± 8.4 | 070 ± 10 | 65 ± 12 | M |
| CE Almoyas | 343 ± 7.8 | 101 ± 10 | 55 ± 5.1 | M |
| CH Almoyas | 333 ± 9.1 | 086 ± 10 | 60 ± 7.7 | M |
| CJ | | 079 ± 10 | 34 ± 12.6 | |
| CK Serrata | 346 ± 9.9 | 074 ± 10 | 20 ± 8.7 | M |
| CM Gabar | 287 ± 14.4 | 051 ± 10 | 47 ± 5.3 | M |
| DF | | 070 ± 10 | 96 ± 9 | |
| S11/DA | | 100 ± 10 | 96 ± 14.2 | |
| Salada mean | 295 ± 4.8 | 030 ± 9.6 | 7 ± 14 | TP |
| B123/4 Engarbo | | 067 ± 10 | 62 ± 7 | |
| S4/K48 | 342 ± 12 | 103 ± 10 | | M |
| S70/K127 | 334 ± 6.7 | 084 ± 10 | | M |
| S56/K6 | 341 ± 10 | 086 ± 10 | | M |
| S75/K13 | 351 ± 8 | 081 ± 10 | | M |
| S34/K133 | 326 ± 8.8 | 035 ± 10 | | M |
| S51/K102 | 336 ± 7.6 | 072 ± 10 | | M |
| S10/K24A | 341 ± 9 | 056 ± 10 | | M |
| S84/K305 | 318 ± 8 | 028 ± 10 | | M |
| SBFT 2,4 | 306 ± 5.6 | 050 ± 10 | | TP |
| SBFT 5–10 | 330 ± 9.5 | 061 ± 10 | | TP |
| SBFT 14 | 311 ± 15.2 | 044 ± 10 | | TP |
| | | *Western Subbetics* | | |
| Sierra Gorda LJ | 290 ± 10 | 348 ± 10 | −7 ± 8.7 | ESP94 |
| NF El Chorro | | 076 ± 10 | 74 ± 13 | |
| NM El Chorro | | 063 ± 10 | 37 ± 12 | |
| NA El Chorro | 294 ± 10 | 043 ± 10 | 69 ± 18 | M |
| ND El Chorro | 308 ± 5.8 | 063 ± 10 | 46 ± 13 | M |
| NG El Chorro | 307 ± 10 | | 62 ± 17 | M |
| NI El Chorro | | 062 ± 10 | 58 ± 17 | |
| RJ02 Blanquilla | 299 ± 5 | 022 ± 10 | 45 ± 7.3 | KP |
| RJ12 Alpandeire | 301 ± 8 | 039 ± 3 | 58 ± 9.1 | KP |
| RC9 Atajate | 290 ± 7.6 | 032 ± 19.9 | 55 ± 5.1 | P95 |
| N Puerto Viento | 294 ± 7 | 027 ± 5 | | KP |
| Cancha de Almola | 293 ± 9 | 045 ± 5 | | KP |
| Carboneras window | 306 ± 10 | 050 ± 10 | | KP |
| N Villaluenga | 292 ± 7 | 022 ± 10 | | KP |
| S Villaluenga | 332 ± 12 | 072 ± 8 | | KP |
| Peñon de Benadalid | 287 ± 10 | 033 ± 10 | | KP |
| N Gaucín | 292 ± 12 | 004 ± 8 | | KP |
| RC11 | 291 ± 11.3 | | 48 ± 12.2 | P95 |
| CF2 | 292 ± 9.3 | 039 ± 7.6 | | P95 |
| CF5 B304/5 | 294 ± 11.5 | 063 ± 5.8 | 67 ± 4 | P95 |
| CF6 B306 | 291 ± 14.6 | | 60 ± 17 | P95 |
| S Gaucin B307 | 250 ± 13.1 | 336 ± 8.5 | 17 ± 13 | P95 |
| S Gaucin B308 | 239 ± 10.3 | 329 ± 7.9 | 22 ± 11 | P95 |
| CF11 B309 | 293 ± 8.2 | 027 ± 7.3 | 68 ± 12 | P95 |
| Sierra Fantasia RC10 | 272 ± 15.6 | 007 ± 10 | 59 ± 7.6 | P95 |
| Los Canutos CC2 | 306 ± 8.8 | 346 ± 12 | 40 ± 4.1 | P95 |
| | | *External Rif* | | |
| Beni Ider | | 340 ± 15 | 41 ± 7.5 | |
| Oued Meshtek | 146 ± 19.5 | 245 ± 15 | | PPO |
| Cherafat | 194 ± 11 | 270 ± 10 | | PPO |
| Sidi Redouane | 232 ± 8 | 355 ± 10 | | TP |
| Mjaara R17–18 | 177 ± 5.4 | 302 ± 10 | −81 ± 9.9 | TP |
| Beni Ouassal R9 | | 345 ± 10 | 12 ± 4.8 | |
| Aïn Lihamdi R7 | | 311 ± 10 | −25 ± 7.7 | |
| Derdaka R8 | | 270 ± 10 | −94 ± 11.3 | |
| Tem bou Zid R6 | | 262 ± 10 | −84 ± 10.5 | |
| Sof Aouzzai R27–28 | | 247 ± 10 | −137 ± 11.3 | |
| Chorfa El Olia | 182 ± 20 | 260 ± 10 | | TP |
| Er Merhour | 198 ± 11.3 | 298 ± 10 | | TP |
| Azrou Akchar | 147 ± 16.1 | 242 ± 20 | −69 ± 6.8 | TP |
| Hajra Ali R31–35 | 165 ± 14.7 | 225 ± 10 | −42 ± 16.6 | TP |

[a]SV, slip vector; *R*, vertical axis rotation. Errors are 95% confidence limits on Fisher mean. Structural trends determined from kilometer-scale folds and thrust traces related to the main phase of contractional deformation and thrusting, and a nominal uncertainty of ±10°, except for some sites where sufficient field measurements were available for Bingham statistics. Sources for kinematic data: TP, this paper; Pz94, *Platzman* [1994]; KP, *Kirker and Platt* [1998]; LPG, *Lonergan et al.* [1994]; M, *Mayfield* [1999]; P95, *Platt et al.* [1995]; PPO, *Platzman et al.* [1993].

12 and 20 measurements were normally made at an observation site, and the mean vector and 95% confidence cone around the mean were calculated. Most data sets show as much variation in plunge (due to variations in the dip of individual slip surfaces) as in trend, and the data are polar in nature, since they relate to a slip direction, so the data were analyzed using Fisher statistics [*Fisher*, 1953]. This also facilitates comparison of the kinematic and paleomagnetic data sets. In some cases, data from several sites within an area of a few square kilometers have been grouped together and the mean value has been quoted. Plunges are generally shallow, so only the slip vector azimuths are given in Table 1.

[16] A second crucial data set presented here consists of estimates of shortening around the arc of the external thrust belt. These were determined by the restoration of structural cross sections. The sections were constructed using surface data, well data, and seismic information where available, and depth to basement was determined from seismic reflection profiles and gravity modeling. Restoration was carried out using the line balance technique where the data justify this or the area balance technique using stratigraphic thicknesses determined from surface geological and well data [e.g., *Hossack*, 1979]. The nature of the data used in each cross section and the sources of uncertainty are discussed individually for each section. Where possible, the sections were constructed parallel to the local direction of shortening determined from the kinematic data; where this was not possible (due to the orientation of seismic lines, for example), shortening estimates were corrected accordingly. The implications of the shortening data are profound: they allow us to reconstruct the original geometry of the indenting margin of the Alborán Domain and to determine the bulk

rotation of the different sectors of the arc. This then bears importantly on the interpretation of the paleomagnetic data (see below).

### 3.2. Paleomagnetic Data

[17] An important aspect of the kinematic evolution of the external Betic-Rif arc is vertical axis rotation, as revealed by paleomagnetic data [*Osete et al.*, 1989; *Platzman*, 1992; *Platzman et al.*, 1993; *Allerton et al.*, 1993; *Platt et al.*, 1995]. These rotations not only provide essential information on the pattern of deformation around the arc but also raise questions about the significance of the kinematic data. If rocks can be rotated during deformation through large angles about vertical axes, then clearly the same is true of the structures within them. Serious consideration of this problem is therefore an important element of this study. Most of the paleomagnetic measurements discussed here have already been published, and the cited papers provide details of sampling and measurement procedures. New data are indicated as such in Tables 2 and 3, and further documentation of these sites is provided in the auxillary data sets.[1] All sampling sites were located in limestones of either Middle to Late Jurassic or Late Cretaceous age. In several cases we have used the mean of two or more sites to constrain the average vertical axis rotation of a fault block or thrust slice: the number of sites and the total number of samples used for the statistical analysis are indicated in Tables 2 and 3.

[18] At most sites, either two or three separate magnetic remanence vectors can be identified: these may include a viscous component induced by the present-day magnetic field that can be removed by demagnetization at temperatures up to around 300°C, an intermediate component stable up to around 450°C, and a high-temperature component (removed at temperatures up to 600°C). Because of the small size and large number of the differentially rotated thrust blocks and fault slices, it has not been possible to carry out rigorous tests of the ages of these remanences for each block. Where these tests have been applied [*Osete et al.*, 1989; *Platzman*, 1992; *Platzman and Lowrie*, 1992; *Allerton et al.*, 1993; *Allerton*, 1994; *Villalaín et al.*, 1994], the high-temperature remanence appears to be essentially primary, produced during deposition or diagenesis, and the intermediate-temperature remanence is interpreted as an overprint produced during deformation, probably as a result of tectonically driven fluid migration [e.g., *Gray and Stamatakos*, 1997]. The tests that have been applied at each site or group of sites are indicated by the following letters in Table 2. The classical fold test (*F*), applied to folds known to be related to the main contractional phase of deformation, demonstrates that the remanence is older than contraction. The regional fold test (*T*), which demonstrates that the remanences from several sites cluster better after correction for the local dip, is a cruder but still useful criterion. Where an intermediate temperature component of magnetization has been identified with a statistically significant difference in declination from the high-T component (*M*), this suggests that the high-T component is likely to be primary, though we note that in the Rif there locally appears to be more than one syndeformational remanence. *R* indicates that one or more samples from a site show reversed polarity: this is provides circumstantial evidence that the remanence is primary because the intermediate-temperature component associated with the tectonic overprint is reported to show uniformly normal polarity [*Allerton et al.*, 1993, *Villalaín et al.*, 1994]. *S* (for Betic samples) indicates that Jurassic and Late Cretaceous sites in the same structural block show a declination difference corresponding to the mid-Cretaceous rotation of Iberia [*Platzman and Lowrie*, 1992]: if they do, the remanences are likely to be primary.

[19] The magnetic declinations, after correction for tectonic tilt, have been converted to rotations relative to geographic north by correcting them for the expected directions for locations within the Iberian or African plates, calculated from the published Late Jurassic, Late Cretaceous, and Miocene virtual geomagnetic poles for these plates [*Westphal et al.*, 1986; *Besse and Courtillot*, 1991]. The reference directions used are listed in Table 2.

## 4. Prebetic Arc

[20] We start the discussion with an analysis of the Prebetic arc: a relatively small-scale arcuate structure within the External Zones of the eastern Betic Cordillera (Figure 3). This structure encapsulates some of the problems of arcuate thrust belts and because of its good exposure and well-constrained geometry allows us to reach some robust conclusions about its development. The arc is developed in a continental to shallow marine Mesozoic and Tertiary sedimentary succession that was deposited on the southern margin of the Iberian platform. The External Prebetic, to the west and north, is characterized by a thin and incomplete succession dominated by Triassic continental clastics and Jurassic platform facies carbonates, whereas the Internal Prebetic has a much thicker and more complete succession and shows transitions to more open marine facies [*García-Hernandez et al.*, 1980]. The external margin of the Prebetic in the west is a sharp thrust front against the late Miocene sediments of the Guadalquivir foreland basin. Farther east it is more diffuse, and there is a poorly defined transition into the folded region of the roughly coeval Iberian Ranges. The internal margin of the Prebetic is defined by the Subbetic Frontal Thrust. Biostratigraphic ages from preorogenic, synorogenic, and postorogenic marine sediments shown on the 1:50,000 geological map sheets published by the Instituto Geologico y Minero de España show that thrusting and folding in the Prebetic took place between the late Burdigalian (about 16 Ma) and the late Tortonian (about 7 Ma).

[21] Structural trends in the External Prebetic swing through ~90° around the Alcaraz antitaxis into the Cenajo syntaxis (Figure 3). Toward the Internal Prebetic, the NW

[1] Auxiliary data sets and figures are available via Web browser or via Anonymous FTP from ftp://agu.org, directory "apend" (Username = "anonymous", Password = "guest"); subdirectories in the ftp site are arranged by paper number. Information on searching and submitting electronic supplements is found at http://www.agu.org/pubs/esupp_about.html.

**Table 2.** Paleomagnetic Data Summary[a]

| Site | *N*/*n* | Age | *D*/*I* | $\alpha_{95}$ | Test | RD/I | *R* | Map | Grid Ref | Ref | Figure 1 |
|---|---|---|---|---|---|---|---|---|---|---|---|
| | | | | | *Eastern Subbetics* | | | | | | |
| B49 Prebetic | 1/9 | LJ | 327/48 | 6.4 | R | 337/35 | −10 | 888 | 7103/4104 | A93 | ✓ |
| B33 Archivel | 1/13 | LJ | 034/51 | 12.5 | R | 337/35 | 57 | 910 | 7493/3964 | A93 | ✓ |
| B34 Archivel | 1/6 | LJ | 354/29 | 20.6 | R | 337/35 | 17 | 910 | 7496/3966 | A93 | ✓ |
| B404/5 Ponce | 2/22 | LJ | 358/34 | 8 | FR | 337/35 | 21 | 932 | [b] | A93 | ✓ |
| All Almirez | 4/29 | LJ | 322/43 | 5.8 | TR | 337/35 | −15 | 952 | [b] | A93 | |
| Burete | 3/27 | LJ | 323/35 | 15.3 | FR | 337/35 | −14 | 911 | [b] | A94 | ✓ |
| Quipar SE | 3/13 | LJ | 031/56 | 16.3 | TR | 337/35 | 54 | 911 | [b] | A94 | ✓ |
| B38–39 Mojantes | 2/15 | LJ | 012/24 | 5 | FR | 337/35 | 35 | 910 | [b] | A93 | ✓ |
| All Salada | 4/34 | LC | 006/39 | 14 | F | 359/55 | 7 | 931 | [b] | ARP | ✓ |
| B123/4 | 2/18 | LJ | 039/31 | 7.3 | T | 337/35 | 62 | 952 | [b] | A93 | ✓ |
| Gabar mean | 10/111 | LC | 055/37 | 8 | R | 359/55 | 56 | 952 | [b] | M | ✓ |
| Maria/Muela mean | 5/31 | LJ | 088/41 | 12 | R | 337/35 | 74 | 952 | [b] | M | ✓ |
| AA Almirez | 1/6 | LJ | 343/37 | 13.4 | R | 337/35 | 6 | 952 | 7533/3607 | M | ✓ |
| CA Alcaide | 1/12 | LC | 048/37 | 10.3 | | 359/55 | 49 | 952 | 7405/3584 | M | |
| CB Gabar | 1/13 | LC | 062/37 | 5.5 | | 359/55 | 63 | 952 | 7348/3527 | M | |
| CC | 1/15 | LC | 064/43 | 12 | | 359/55 | 65 | 952 | 7356/3562 | M | |
| CE Almoyas | 1/7 | LC | 054/41 | 5.1 | | 359/55 | 55 | 952 | 7413/3552 | M | |
| CH Almoyas | 1/8 | LC | 059/33 | 7.7 | R | 359/55 | 60 | 952 | 7393/3560 | M | |
| CJ | 1/10 | LC | 033/25 | 12.6 | R | 359/55 | 34 | 952 | 7371/3579 | M | |
| CK Serrata | 1/9 | LC | 019/31 | 8.7 | | 359/55 | 20 | 952 | 7479/3596 | M | |
| CM Gabar | 1/12 | LC | 046/43 | 5.3 | F | 359/55 | 47 | 952 | 7354/3529 | M | |
| DF | 1/10 | MJ | 074/53 | 9 | | 338/41 | 96 | 952 | 7243/3428 | M | |
| DA | 1/7 | LJ | 074/64 | 14.2 | | 337/35 | 97 | 952 | 7451/3502 | M | |
| | | | | | *Western Subbetics* | | | | | | |
| JGO1/2 Gorda | 2/19 | LJ | 349/40 | 4.0 | F | 336/35 | 13 | 1025 | [b] | V94 | ✓ |
| Gorda LJ | 5/47 | LJ | 329/34 | 8.7 | TRS | 336/35 | −7 | 1025 | [b] | P94/P92 | ✓ |
| Gorda LC | 1/7 | LC | 009/50 | 6.3 | S | 359/53 | 9 | 1025 | [b] | P94/P92 | |
| NF El Chorro | 1/10 | LJ | 053/51 | 13 | FM | 336/35 | 74 | 1038 | 5063/2594 | M | |
| NM El Chorro | 1/11 | LJ | 013/23 | 12 | R | 336/35 | 37 | 1038 | 5098/2599 | M | |
| NA El Chorro | 1/13 | LJ | 045/52 | 18 | | 336/35 | 69 | 1038 | 5024/2596 | M | |
| ND El Chorro | 1/15 | LJ | 022/43 | 13 | M | 336/35 | 46 | 1038 | 5084/2604 | M | |
| NG El Chorro | 1/10 | LJ | 038/53 | 17 | | 336/35 | 62 | 1038 | 5064/2634 | M | |
| NI El Chorro | 1/17 | LJ | 034/27 | 17 | | 336/35 | 58 | 1038 | 5080/2621 | M | |
| All El Chorro | 10 | LJ | 033/41 | 9 | | 336/35 | 65 | 1038 | [b] | M | ✓ |
| 3 Archidona | 1/7 | LJ | 043/54 | 6.0 | | 336/35 | 67 | 1024 | [b] | PL92/ESP92 | ✓ |
| 4 Antequera | 4/37 | LJ | 036/43 | 10.3 | | 336/35 | 60 | 1038 | [b] | PL92/ESP92 | ✓ |
| 5 Teba LJ | 1/8 | LJ | 044/50 | 5.70 | S | 336/35 | 68 | 1037 | [b] | PL92/ESP92 | |
| 6 Teba LC | 1/9 | LC | 073/21 | 5.9 | S | 359/53 | 74 | 1037 | [b] | PL92/ESP92 | ✓ |
| 7 Puerto de Venta | 3/25 | LJ | 036/51 | 12.36 | S | 336/35 | 60 | 1051 | [b] | PL92/ESP92 | |
| 8 Puerto de Venta | 3/32 | LC | 056//41 | 5.8 | S | 359/53 | 57 | 1051 | [b] | PL92/ESP92 | ✓ |
| 9 Ubrique | 6/49 | LJ | 042/44 | 13.0 | S | 336/35 | 66 | 1050 | [b] | PL92/ESP92 | |
| 10 Ubrique | 5/48 | LC | 061/36 | 11.1 | RS | 359/53 | 62 | 1050 | [b] | PL92/ESP92 | ✓ |
| RJ02 Blanquilla | 1/7 | LJ | 021/47 | 7.3 | S | 336/35 | 45 | 1051 | [b] | PL92 | |
| RJ12 Alpandeire | 1/10 | LJ | 034/38 | 9.1 | | 336/35 | 58 | 1065 | [b] | PL92 | |
| B304 Guadiaro | 11 | LC | 062/35 | 4 | F | 359/53 | 63 | 1064 | 2881/0496 | P95 | ✓ |
| B305 Guadiaro | 11 | LC | 074/46 | 5 | F | 359/53 | 75 | 1064 | 2881/1496 | P95 | |
| B306 | 8 | LC | 059/22 | 16 | | 359/53 | 60 | 1064 | 2904/0504 | P95 | |
| B309 | 11 | LC | 067/50 | 10 | | 359/53 | 68 | 1064 | 2912/0537 | P95 | |
| RC11* | 10 | LC | 047/30 | 9 | | 359/53 | 48 | 1064 | 2902/0490 | P95 | |
| RC10 Fantasia | 11 | LC | 059/40 | 8 | | 359/53 | 59 | 1064 | 2767/0479 | P95 | ✓ |
| B307 | 15 | LC | 016/53 | 10 | R | 359/53 | 17 | 1064 | 2889/0433 | P95 | |
| B308 | 11 | LC | 021/45 | 10 | F | 359/53 | 22 | 1064 | 2899/0433 | P95 | |
| RC09 | 10 | LC | 055/42 | 5 | | 359/53 | 56 | 1064 | 3001/0587 | P95 | |
| CC02 Canutos | 9 | LC | 039/51 | 4 | | 359/53 | 40 | 1071 | 2965/0328 | P95 | ✓ |
| | | | | | *External Rif* | | | | | | |
| R1–3,29,30 Akchar | 43/5 | EJ | 291/43 | 6.8 | F* | 000/44 | −69 | TO | 6432/4652 | T3 | ✓ |
| R31–35 Hajra Ali | 5/28 | EJ | 318/39 | 16.6 | | 000/44 | −42 | TO | 6413/4637 | T3 | ✓ |
| R27–28 Sof Aouzzai | 1/9 | EJ | 223/37 | 11.3 | F* | 000/44 | −137 | DS | 6009/4569 | T3 | ✓ |
| R6 Tem bou Zid | 1/11 | EJ | 276/39 | 10.5 | | 000/44 | −84 | DS | 5887/4540 | T3 | ✓ |
| R7 Aïn Lihamdi | 1/10 | EJ | 312/39 | 7.7 | | 337/43 | −25 | TF | 5237/4369 | T3 | |
| R8 Derdaka | 1/9 | EJ | 243/50 | 11.3 | | 337/43 | −94 | TF | 5223/4379 | T3 | ✓ |
| R9 Beni Ouassal | 2/13 | EJ | 349/33 | 4.8 | F | 337/43 | 12 | TF | 5215/4387 | T3 | ✓ |
| R17–19 Mjaara | 2/22 | EJ | 279/69 | 9.9 | | 000/44 | −81 | TF | 5154/4433 | T3 | ✓ |
| TC01 Beni Ider | 1/9 | LC | 023/45 | 7.5 | | 342/38 | 41 | M | [b] | PPO93 | ✓ |

**Table 3.** New Paleomagnetic Data From the Rif[a]

| Location | Before Correction | | | After Correction | | | | | |
|---|---|---|---|---|---|---|---|---|---|
| | *D*/*I* | *K* | $\alpha_{95}$ | *D*/*I* | *K* | $\alpha_{95}$ | *n* | Bedding Dip/Direction* | Analysis |
| R1–3,29,30 Akchar | 291/43 | 11.4 | 6.8 | 307/41 | 6.1 | 11.4 | 43 | 46/171 (R3) | LR |
| R31–35 Hajra Ali | 318/39 | 3.5 | 16.6 | 155/72 | 3.9 | 15.3 | 28 | 48/136 (R32) | GC |
| R27–28 Sof Aouzzai | 223/64 | 21.6 | 11.3 | 292/37 | 10.9 | 16.3 | 9 | 64/326 | LR |
| R6 Tem bou Zid | 276/39 | 20.9 | 10.5 | 232/29 | 20.9 | 10.2 | 11 | 59/172 | LR |
| R7 Aïn Lihamdi | 279/23 | 40.3 | 7.7 | 312/39 | 40.3 | 7.7 | 10 | 53/041 | LR |
| R8 Derdaka | 221/32 | 21.7 | 11.3 | 243/50 | 21.7 | 11.3 | 9 | 30/356 | LR |
| R9,20 Beni Ouassal | 316/44 | 8.3 | 15.3 | 349/33 | 22.2 | 4.8 | 13 | 60/020 (R9) | LR |
| R17–19 Mjaara | 279/69 | 10.1 | 9.9 | 160/−73 | 7.0 | 12.6 | 22 | 19/042 | GC |

[a]*D*, mean declination; *I*, mean inclination; *K*, precision factor; *n*, number of samples used in analysis. Analysis: LG, linear regression; GC, great circle. Bedding dip and dip direction given for single site localities, or a representative site (in parentheses) for multisite localities.

trending sector between these two arcs is progressively replaced by the dextral Socovos fault, which transfers some of the displacement southeastward across the Subbetic at least as far as the IEZB (Figure 1). The structural style also changes markedly around these major swings in trend: in the NE trending Cazorla sector the shortening has mainly been taken up by west directed thrusting, whereas in the NW trending Elche sector, large-scale folding is more important and forethrusts and back thrusts are about equally developed.

[22] Fault slip vectors azimuths change trend markedly around the arcuate structures (Figure 3). There is strong correlation between the slip vectors and the local trend of folds and thrusts, with the slip vectors trending nearly normal to the structural trends (Figure 4). The best indicator of the degree of correlation between two data sets, both of which are subject to observational error, is the slope of reduced minimum axis [*Davis*, 1986], which is shown on Figure 4. The slope is, in fact, >1 (1.28 ± 0.08), which reflects high variance of the data.

[23] To investigate the role of vertical axis rotations, we took samples for paleomagnetic analysis from 16 sites, covering much of the region and most of the stratigraphic units. Unfortunately, only one site (B49) gave useable data (Figure 3): this was taken in a rare exposure of Late Jurassic *ammonitico rosso* facies limestone [*Allerton et al.*, 1993]. The results indicate that there has been little or no vertical axis rotation (Table 2).

[24] We determined the amounts of shortening across the Prebetic by restoration of three cross sections, with the aim of restoring the prethrusting geometry of the region and elucidating the origin of the arcuate structure. Depth to the Iberian basement was constrained by gravity modeling [*Mandeville*, 1993] and stratigraphic thicknesses from surface geological and well data [*Banks and Warburton*, 1991]. Estimated stratigraphic thicknesses taper from 3100 m in the Internal Prebetic through 1120 m in the External Prebetic to 600 m on the external margin of the thrust belt. There is no evidence for involvement of the Iberian basement in Alpine tectonics, and the widespread exposure of the Triassic evaporitic succession at the base of thrust slices and in anticlinal fold cores suggests that this was the level of the basal decollement. Cross sections were constructed by line balancing on the Jurassic limestone. Quoted uncertainties in the shortening estimates arise mainly from the uncertainty of ±500 m in the depth to basement at the rear of the section, as determined by gravity modeling. Very little uncertainty arises from erosion off the top of the sections, as indicated by the widespread preservation of predeformational, syndeformational, and postdeformational Miocene sediments.

[25] The largest amount of shortening, 48 ± 11 km, is shown by the Cazorla section (Figure 5). This section extends from the Prebetic Front 21.4 km back to the boundary of the Internal Prebetic (Figure 3) and was constructed in the direction 300°, close to the mean orientation of the slip vectors in the Cazorla sector (298°). The shortening in the remaining part of the Internal Prebetic was estimated from the cross section by *Banks and Warburton* [1991], constructed along a parallel line, at 4 km. This gives a total of 52 ± 12 km shortening across the Prebetic on a section now 50.4 km long. The Elche section was constructed at 020° in the NW trending sector to the NE of the Socovos fault (Figure 3) and indicates 25 ± 6 km shortening. This section extends 20.9 km from the Socovos fault and was not continued as far as the Prebetic, as the orientation of the slip vectors changes markedly. It is likely to have been affected by out-of-plane motions and possibly vertical axis rotations associated with the Socovos fault, as indicated by the presence of minor strike-slip faults and by

*Notes to Table 2*

[a]*N*, number of sites per locality; *n*, total number of samples. Rock ages are EJ, Early Jurassic; MJ, Middle Jurassic, LJ, Late Jurassic; LC, Late Cretaceous. *D*, mean declination; *I*, mean inclination, after structural corrections. Tests are *F*, fold; *F** failed fold test; M, multicomponent; R, reversal; S, predicted difference in declination between Jurassic and Cretaceous sites in Iberia; T, tilt. RD/I, reference declination and inclination calculated for location and inferred age of remanence from Africa and Iberia poles of rotation [*Besse and Courtillot*, 1991; *Westphal et al.*, 1986]. *R*, vertical axis rotation from reference direction. Map is 1:50,000 geological map sheets published in Spain by Instituto Geologico y Minera de España (by number), in Morocco by Service Géologique du Maroc (DS Dhar Souk; M, Melloussa, TO, Tafrannt de l'Ouerrha, TF, Tizi Ousli). Grid ref is taken from geological map sheets. Data sources are A93, *Allerton et al.* [1993]; A94, *Allerton* [1994]; ARP, *Allerton et al.* [1994]; Pz92, *Platzman* [1992]; Pz94, *Platzman* [1994]; M, *Mayfield* [1999]; PL92, *Platzman and Lowrie* [1992]; PPO, *Platzman et al.* [1993]; P95, *Platt et al.* [1995]; V94, *Villalaín et al.* [1994]; T3, Table 3 this paper. Data shown in Figure 1 indicated in right-hand column.

[b]See indicated data source for multiple site locations.

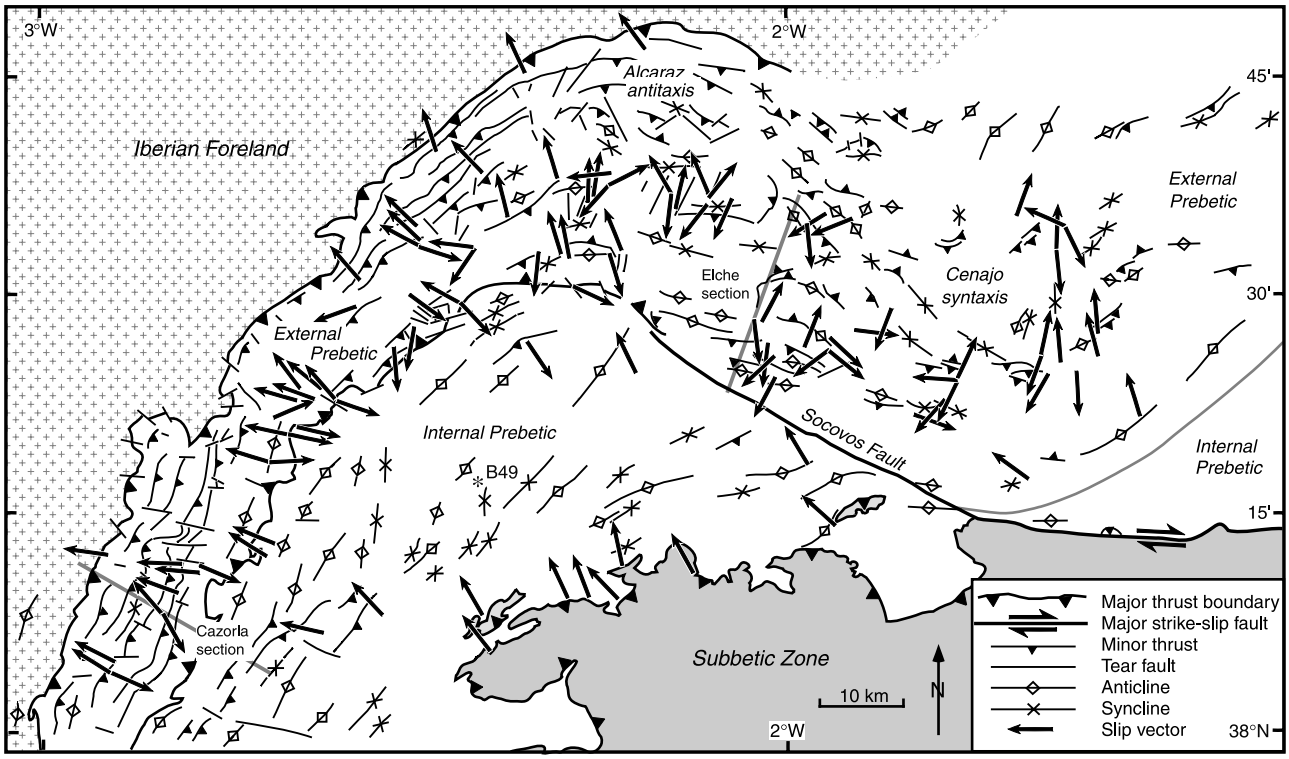


**Figure 3.** Structural map of the Prebetic arc, after *Mandeville* [1993]. Paleomagnetic site B49 is indicated with a star. The Cazorla (Figure 5) and Elche sections are indicated.

the variability in the slip vectors (Figure 3). The Yecla section was constructed at 300° farther east (Y in Figure 1) and indicates 12 ± 5 km of shortening. The shortening direction is not well constrained, but slip vector and stylolite orientations collected by *De Ruig* [1990] in this area lie between 290° and 320°. The section extends for 46.3 km from a region of very low strain in the most external part of the Prebetic to within 15 km of the Subbetic Frontal Thrust. The remaining part of the Internal Prebetic is covered by postorogenic sediment, and we estimate the shortening by extrapolation at ~4 km, giving 16 km total shortening across this part of the Prebetic. Lower and upper uncertainty limits are 7 and 25 km, respectively.

[26] The consistency of the thrust-related slip vectors in the Cazorla sector, the lack of evidence for additional components of deformation, and the paleomagnetic data indicating a lack of vertical axis rotation all suggest that the overall shortening direction indicated by the data in that sector (300°) should be taken at face value. This is close to the trend of the Socovos fault, which transferred the displacement SE (Figure 6). The Elche section, however, taken at face value, suggests that the Socovos fault itself has been displaced 25 km NNE relative to the Iberian foreland. This displacement would also have affected the Cazorla section to the SW of the Socovos fault and if added to our shortening estimate for the Cazorla section gives a net displacement of 62 km toward 324° relative to the Iberian foreland. This result conflicts with both the slip vector data from the Cazorla region and the displacement estimated

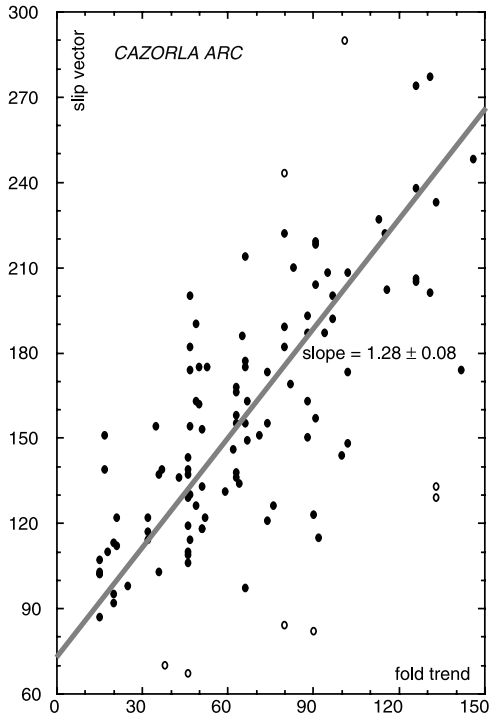


**Figure 4.** Correlation plot of slip vectors against structural trends in the Prebetic arc. Open circles indicate points that were omitted from the regression.

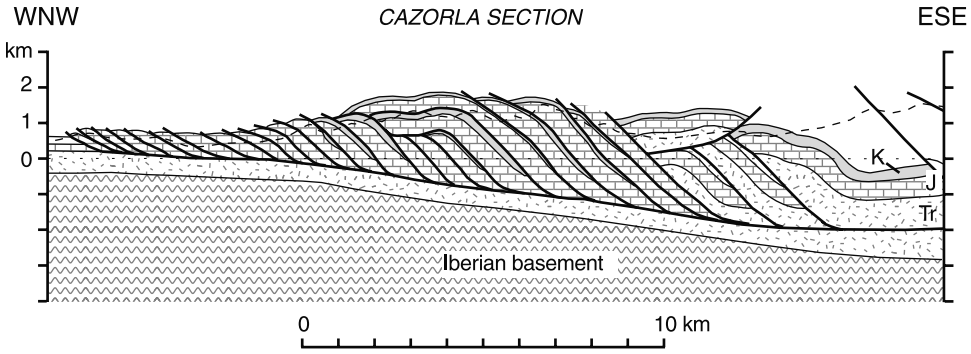


**Figure 5.** Section across the Sierra Cazorla in the Prebetic arc (see Figure 3 for location). Depth to basement was constrained by gravity modeling [*Mandeville*, 1993].

from the restored section. The data from either the Cazorla or the Elche section must therefore be reexamined.

[27] The region of NW trending folds and thrusts in the Elche region is probably a zone of distributed strain associated with the Socovos fault, and significant clockwise vertical axis rotations are therefore likely. In the absence of paleomagnetic data from this region, we can only guess at their magnitude, but a possible indication is the change in orientation of the slip vectors from around 020° in the Elche area to 335° in the outer part of the Alcaraz antitaxis (Figure 3). This suggests that shortening in the Elche section was accompanied by ~45° of clockwise vertical axis rotation and that the original orientation of the restored section was 335°. The restoration in Figure 6 has been carried out on this

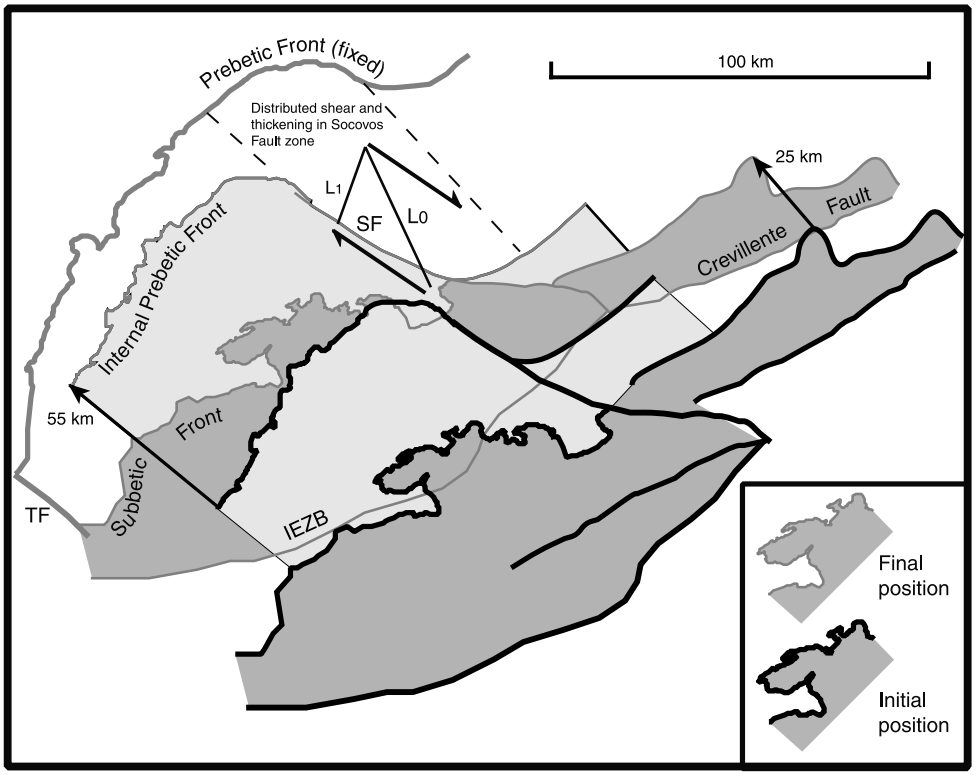


**Figure 6.** Restoration of Prebetic arc to its Burdigalian (early Miocene) configuration. IEZB, Internal-External Zone Boundary; SF, Socovos Fault; TF, Tiscar Fault. See text for discussion of displacement estimates. $L_0$ and $L_1$ indicate initial and final lengths and orientation of material line in Socovos Fault zone parallel to Elche section line, subjected to dextral shear, vertical thickening, and rotation, giving net horizontal shortening of 20 km. Note (1) embayment in restored geometry of Internal Prebetic Front, which is amplified into Prebetic arc; (2) restored position of Subbetic, which lies beneath present-day Internal Zones (where its basement still remains), and (3) restored geometry of Crevillente Fault, which is offset, implying that it was not a throughgoing fault in early Miocene time.

assumption and using the lower limit on the displacement in the Elche section (20 km). This restoration only requires 10 km of displacement of the Socovos fault and the Cazorla section to the NE. The net displacement of the Cazorla section is then 55 km toward 310°. This would imply that there has been either a modest amount of anticlockwise rotation in the Cazorla sector or that there has been a hidden component of strain, possibly in the form of a small amount of sinistral slip along strike-parallel faults.

[28] In restoring the more easterly parts of the Prebetic, we had to use the maximum possible displacement indicated by the Yecla section (25 km, taken to be toward 320°), together with 8° of clockwise rotation, to maintain compatibility with the restored sections to the west. This restoration largely eliminates the deflection of the Subbetic Frontal Thrust across the Socovos fault. It leaves an offset of 22 km in the trace of the Crevillente fault, however, and this is a measure of the amount of dextral displacement that has been transferred from the Cazorla region back to the IEZB. This is probably a minimum value: the choices we have made in restoring the Prebetic have all been designed to minimize incompatibility across the Socovos fault system and, in doing so, have minimized the net displacement transferred to the SE.

[29] The results of our restoration have three very important implications for the origin of the arcuate structures in the Prebetic, and for the Miocene evolution of the eastern Betic Cordillera as a whole.

[30] First, the Internal-External Prebetic Boundary after restoration has a deflection of ~49 km, implying that the fault was localized along a preexisting structure, established perhaps during Mesozoic rifting. The arcuate structure therefore reflects a preexisting embayment in the Iberian platform. As the orogenic front advanced NW, the Socovos transfer fault initiated along the NE side of the embayment, creating a zone of NW trending folds associated with substantial vertical axis rotations. The divergent pattern of slip vectors around the arc is likely to be primarily a result of vertical axis rotation in this zone of distributed shear, with partitioning of deformation across the Socovos fault playing a minor role.

[31] Second, 24 km of displacement along the Socovos fault was transferred into the area from the Internal Betics, which implies that late Miocene shortening in the easternmost Internal Betics was directly linked to deformation in the Prebetic arc.

[32] Third, our estimated offset of 22 km in the restored position of the Crevillente Fault implies that it did not exist as a throughgoing structure prior to the late Miocene deformation in the Prebetic and the displacement on the Socovos Fault.

## 5. Subbetic Zone

[33] We continue the discussion with data from the Subbetic Zone, which extends the whole length of the Betic Cordillera and swings into the main arc by Gibraltar. The zone consists of deformed Mesozoic-Paleogene sequences deposited in a series of complex rift basins on the southern margin of Iberia. The present-day structural complexity makes reconstruction of the paleogeography difficult, and assignments of particular regions to paleogeographic domains tend to be model-dependent, introducing an element of circularity into arguments. The general consensus is that there are three main paleogeographic domains: External Subbetic, comprising platform facies Jurassic carbonates and a thin Cretaceous sequence; Median Subbetic, characterized by deep basinal deposition including calciturbidites, slumps, and debris flows from the surrounding platforms; and Internal Subbetic, characterized by carbonate platform deposition in the Jurassic (including condensed and hardground facies), substantial hiatuses in the Early Cretaceous, and pink pelagic limestones and marlstones in the Late Cretaceous [*Hermes*, 1978; *García-Hernandez et al.*, 1980]. An "Intermediate Zone" basin separating the Subbetic from the Prebetic is also recognized in places.

[34] Miocene deformation in the Subbetic was thin skinned: there is no evidence for involvement of the underlying Iberian basement. The structural geometry is characteristically irregular, with discontinuous internally folded and imbricated slabs of platform facies Jurassic limestone dispersed in a poorly exposed terrain of Triassic evaporites and marlstones and Cretaceous to Paleogene marlstone and marly limestone. Folds and thrusts have locally very variable orientations, and steep discontinuous strike-slip and normal faults with variable trends are common. This structural style is partly a result of Mesozoic extensional tectonics: in common with much of the Tethyan area [*Bernoulli and Jenkyns*, 1974] the Early Jurassic carbonate platforms that formed on what became the southern margin of Iberia were broken up by rifting later in the Jurassic and Early Cretaceous [*Comas et al.*, 1986; *Reicherter et al.*, 1994; *Vera*, 1983]. Extension was accompanied by substantial sinistral shear along the Africa-Iberia plate boundary [e.g., *Dewey et al.*, 1989], and the normal-fault-bounded blocks that formed at this time have an approximately N-S trend in present-day coordinates. These normal faults have commonly been reactivated by later thrusting and strike-slip faulting, but the fault blocks and the breccias and conglomerates that were shed from them from Late Jurassic to Oligocene time can be identified in various places [e.g., *Allerton et al.*, 1994; *Mayfield*, 1999; *Rey*, 1998].

[35] Vertical axis rotation is another factor that has contributed to the irregular structural style of the Subbetic: thrusting was commonly accompanied by ~60° of clockwise rotation [*Platzman and Lowrie*, 1992]. In the eastern Subbetic the amount of rotation is very variable, and some blocks have rotated through angles possibly exceeding 180° [*Allerton et al.*, 1993]. This has clearly contributed to the irregular shapes and discontinuous nature of the Jurassic slabs and the variable trends of the structures.

[36] There are large exposure areas of Triassic rocks that have the aspect of a mélange, consisting of blocks a few centimeters to a few kilometers in extent of bedded Triassic dolostone, altered basaltic pillow lava or dolerite, and

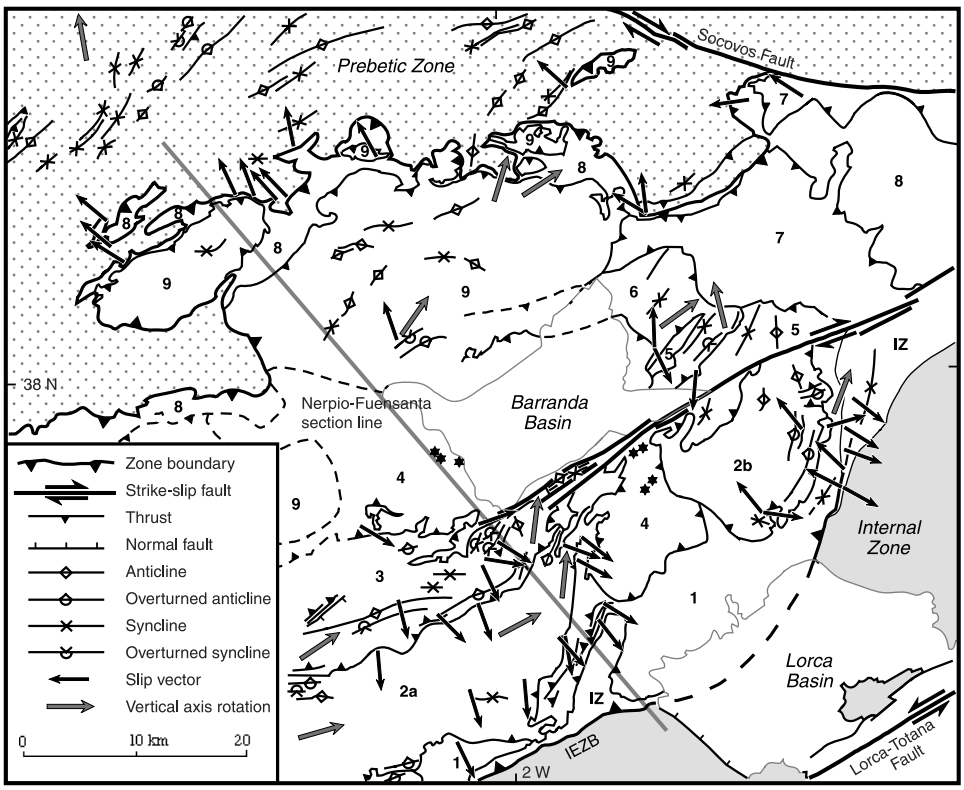


**Figure 7.** Structural map of part of eastern Subbetic Zone with representative kinematic and palaeomagnetic data. Individual thrust sheets numbered as follows: IZ, Tertiary clastic sediments with Internal Zone boundary; 1, Internal Subbetic Late Cretaceous and Tertiary; 2, Internal Subbetic, mainly Jurassic; 2a, Sierra Maria/Almirez sheet; 2b, Sierra de Ponce sheet; 3, Median Subbetic Cretaceous and Tertiary; 4, 5, 7, Triassic; 6, Median Subbetic Jurassic to Tertiary; 8, External Subbetic Cretaceous; 9, External Subbetic Jurassic. Paleomagnetic arrows indicate vertical axis rotation relative to Iberian reference direction for age of rock. Stars indicate locations of isolated blocks along Crevillente fault zone showing very large rotations. Nerpio-Fuensanta section (Figure 8) is indicated.

foliated gypsum or anhydrite, in a gypsiferous matrix. Irregular blocks of Jurassic to Miocene rocks are also surrounded by the mélange. *De Smet* [1984] interpreted this block-in-matrix mélange in the eastern Subbetic as the product of extensive dextral shear along the Crevillente fault zone (Figure 1). It is likely that the mélange reflects mobility of the Triassic evaporitic sequence throughout its history, and in particular during the Mesozoic rifting as well as during Neogene thrusting and strike slip. The mélange is distributed as sheet-like bodies over large areas of the Subbetic, not just in the vicinity of strike-slip faults.

### 5.1. Eastern Subbetic

[37] The region we have studied (Figure 7) is contiguous with the Prebetic arc and with it forms a transect extending from the Iberian foreland to the Internal/External Zone Boundary. It is dominated by four major tectonic features.

[38] 1. In the north, the Subbetic Frontal Thrust (SFT) has translated the Subbetic as a whole ~40 km NW onto the Prebetic [*Banks and Warburton*, 1991].

[39] 2. The SFT is replaced to the east as the main Subbetic/Prebetic boundary by the eastern continuation of the Socovos Fault, which offsets the SFT by ~25 km.

[40] 3. To the southeast, the Subbetic is delimited by the Internal/External Zone Boundary (IEZB), which in this region is a backthrust that has allowed the Internal Zones to move roughly NW beneath the Subbetic [*Lonergan et al.*, 1994]. The thrust overrides Burdigalian (early Miocene) sediment and is overlapped by Langhian (middle Miocene) sediment, providing a very tight constraint on its timing [*Lonergan et al.*, 1994; *Geel and Roep*, 1999]. It appears that as the Internal Zone wedge moved onto the Iberian margin in the eastern Betics, it moved along a major decollement near the base of the Mesozoic sequence, and a blind front developed linking this forethrust with a backthrust that allowed it to move beneath the main body of the Subbetic (Figure 8). This blind front probably emerges at the present erosion level north of Granada, as from this point west the IEZB is a WNW directed forethrust.

[41] 4. The Subbetic Zone is roughly bisected by the Crevillente Fault. This is a very clearly defined lineament trending 070° for 150 km west from Alicante (Figure 1). On

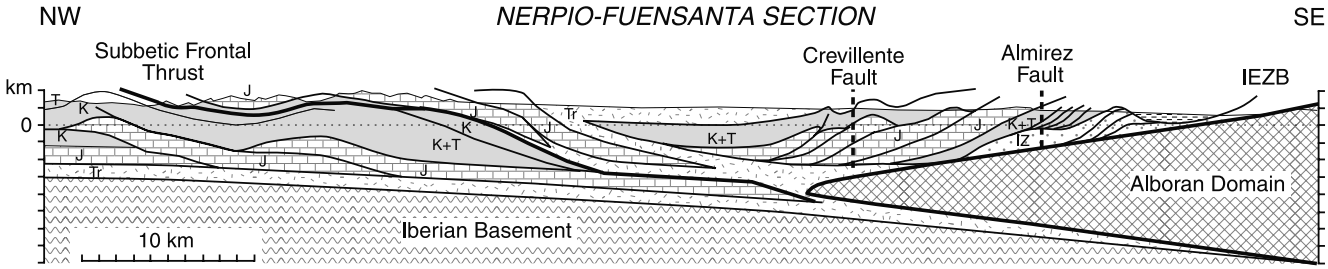


**Figure 8.** Nerpio-Fuensanta section (eastern Subbetic, see Figures 1 and 7 for location). The Crevillente and Almirez faults produce displacements out of plane of section. Structure at depth is constrained by seismic profiles [*Banks and Warburton*, 1991]; depth to basement is constrained by gravity modeling [*Mandeville*, 1993]. See color version of this figure at back of this issue.

some maps it is shown extending to Cadiz [e.g., *De Smet*, 1984; *Sanz de Galdeano*, 1996], and *De Smet* [1984] has attributed the formation of the entire Betic orogen to dextral slip on this fault. There are no geological markers to indicate the sense or amount of displacement, but kinematic indicators suggest sinistral motion in post-Miocene time [*Bousquet*, 1979]. Where the fault zone cuts early Miocene and older rocks within the area of Figure 7, there is evidence for both sinistral and dextral slip on faults subparallel to the zone as a whole, and this segment of the fault may have been a zone of dextral slip in middle to late Miocene time. It appears to die out westward and cannot be traced as a discrete structure through the region. The absence of any significant change in the geology, the structural style, or the depth of erosion across the fault suggests that the displacement was not large. Pre-Mesozoic basement is never exposed within the Subbetic on either side of the fault, nor is there any expression in the gravity or magnetic field that would suggest that the fault affects the basement. It seems likely, therefore, that it is confined to the Mesozoic and Tertiary cover.

[42] We have recognized a number of major thrust sheets within the eastern Subbetic, which are indicated on the map (Figure 7) and section (Figure 8). The lithological characteristics of these thrust sheets are described in the caption to Figure 7. Each of these sheets is internally folded and some are imbricated. Sheets 4, 5, and 7 are part of an interconnected set of sheets of Triassic mélange that separates the more coherent thrust sheets (Figure 8) and probably accommodated much of the relative motion between them.

### 5.1.1. Nerpio-Fuensanta Cross Section

[43] The lack of long-range structural continuity within the Subbetic, the existence of large vertical axis rotations, and the presence of two major strike-slip faults make the construction of balanced cross sections and the estimation of shortening difficult. The Nerpio-Fuensanta section trends 320°, close to the mean of the present-day slip vectors in the Subbetic (329 ± 3°). The section is based on surface observations, and the depth to basement was constrained by gravity modeling [*Mandeville*, 1993]. Structure at depth is speculative and based in part on the parallel section by *Banks and Warburton* [1991] and is intended to illustrate our understanding of the structural style. The total shortening is 139 km, based on line balancing on the Jurassic limestones. This estimate includes 35.8 km displacement on the Subbetic Frontal Thrust, 26.4 km displacement on the IEZB, and 68.1 km shortening within the Subbetic wedge. Using an area balance approach, the shortening estimate is equivalent to assuming an average stratigraphic thickness for the Subbetic of 1950 m, including the Triassic. The uncertainty on this thickness is ±500 m, giving ±33 km uncertainty in shortening. Note also that the estimated stratigraphic thickness in the Prebetic at the NW end of the section is 3100 m and in the buried Intermediate Zone trough it is up to 4500 m. The uncertainty on the basement depth is 500 m, giving rise to an additional uncertainty in the shortening of 14 km.

[44] The significance of this shortening estimate has to be reconsidered in the light of the evidence for the effect of vertical axis rotation on the orientation of the structures and of the slip vectors, discussed in sections 5.1.2 and 5.1.3.

### 5.1.2. Kinematic Data

[45] Slip vectors from thrusts in the eastern Subbetic are shown on Figure 7 and summarized in Table 1. The data show considerable variability on small spatial scales, but certain features are immediately apparent. The Subbetic Frontal Thrust and the Northern Subbetic show NW directed thrust vectors, and the thrusts are associated with folds that are inclined or overturned to the NW (see also Figure 4b). The mean trend of all slip vector data from the footwall of the SFT is 322° ± 14.5°. Thrust vectors from the Median and Southern Subbetic are mainly SE directed and are associated with folds inclined or overturned to the SE. The IEZB, which forms the southeastern boundary of the Subbetic, is itself a major backthrust with ESE to SSE directed slip vectors (Figure 7). The transition from NW to SE directed thrusting and folding occurs a few kilometers north of the Crevillente fault. On a small scale, both NW and SE directed thrusting occur together in many locations over the whole region, but we have found no evidence that the position of the main changeover from NW to SE directed thrusting migrated with time with respect to the rock mass. The mean trend of fault slip vectors from both NW and SE directed thrusts in the Subbetic is 329° ± 3°.

[46] Disregarding the polarity of thrusting, the trends of the slip vectors as shown on the map (Figure 7) correlate broadly with the structural trend. A correlation plot of slip vectors against structural trend (Figure 9a) brings this out but

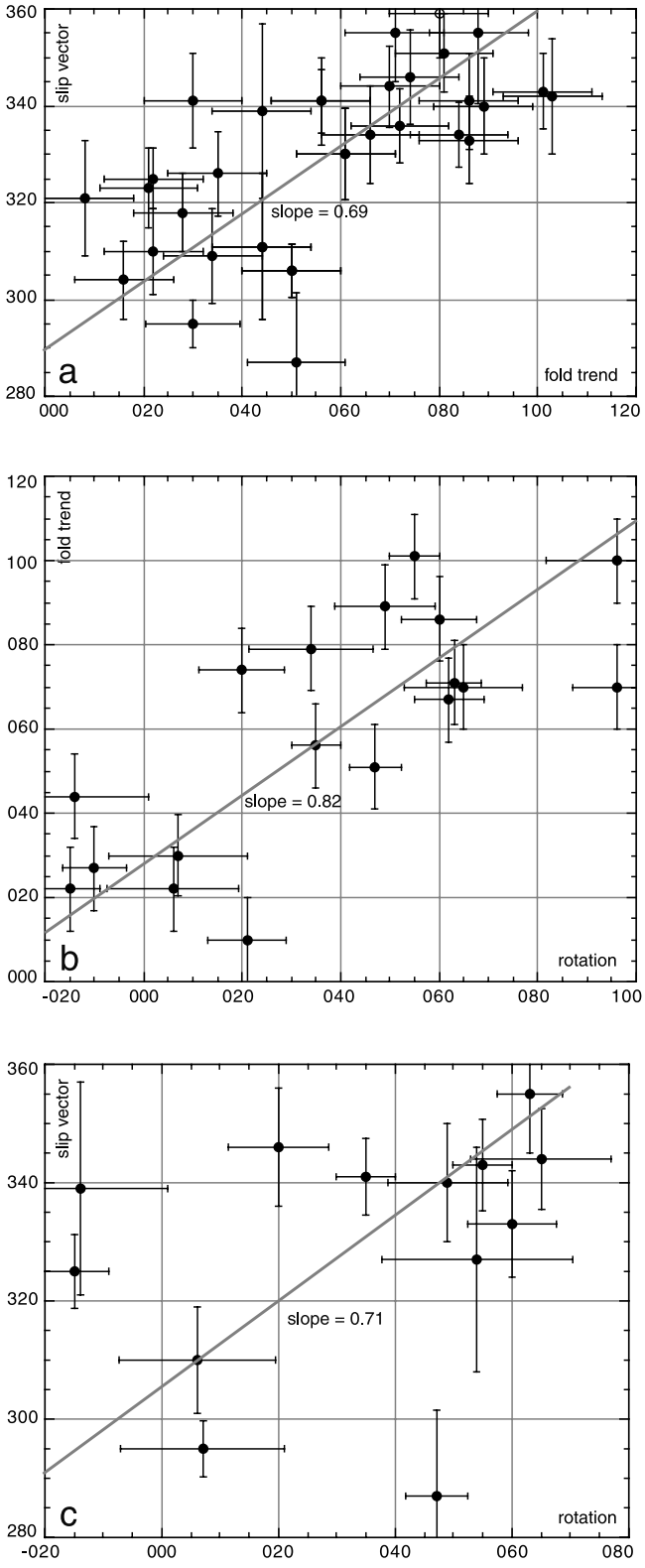


**Figure 9.** Correlation plots for the eastern Subbetic. (a) Slip vectors against fold trends. (b) Fold trends against vertical axis rotations. (c) Slip vectors against vertical axis rotations.

shows that the correlation is partial, with a slope of 0.69 ± 0.9. Note that the slope of the plot indicates the relative rate of change of the two variables: in this case the slip vectors change orientation at only two thirds of the rate that the trend changes. This probably means that at least some of the measured slip vectors formed relatively late in the deformation history, after rotation had started.

[47] The slip vector data from some locations show considerable complexity: multiple sets of lineations within fault zones, overprinting sets of lineations on individual surfaces, and spatial variations in slip vector orientation along major fault zones are common. These variations are likely to reflect both the rotation of previously formed structural features and the spatial and temporal changes in the slip direction associated with vertical axis rotation of the fault blocks during thrusting. These effects have been discussed in some detail by *Allerton* [1994, 1998] and *Kirker and McClelland* [1996]. It has not been possible to show these variations adequately on the map, and some data were excluded from the correlation plots. Specific examples of these variations are presented in the auxiliary data set.

### 5.1.3. Paleomagnetic Data

[48] Paleomagnetic data from the eastern Subbetic are summarized on the map (Figure 7) and in Table 2. The data shown on the map are in most cases averages of more than one site and are shown for illustrative purposes only. The original data and discussions of the age and character of the magnetic remanences are presented by *Allerton et al.* [1993, 1994], *Allerton* [1994], and *Mayfield* [1999]. The paleomagnetic data for the most part indicate clockwise rotations up to ~90°. Larger rotations, up to 180° or more, are shown by some small (kilometer-sized) Jurassic limestone blocks within the Triassic mélange: these have been omitted from the map for clarity, but the locations are indicated by stars on Figure 7. Data from the interiors of large coherent thrust sheets do not exceed 90°.

[49] The data on the map suggest that there is a broad correlation between structural trend and the amount of rotation, and this is borne out by the correlation plot (Figure 9b), which has a slope of 0.82 ± 0.12, with an intercept at zero rotation of 029° ± 10°. This implies that the folds were initiated with a NNE trend and have been rotated into their present trends. There are also marked contrasts in the amount of rotation between adjacent major thrust sheets, and there are significant variations within some thrust sheets. The most dramatic of these is the Burete fold in thrust sheet 6 (B in Figure 7), which shows 68° of clockwise vertical axis rotation of the upper limb relative to the lower limb [*Allerton*, 1994], and within the Sierra Maria/Almirez sheet (thrust sheet 2a in Figure 7), where the rotation increases from around zero to >90° from NE to SW. These features suggest that the rotations were associated with the main contractional phase of deformation, and were mainly accommodated by variations in displacement on the surrounding thrusts. Some blocks have normal or strike-slip faults bounding one or more sides, which may have been formed during rotation, but this is not systematically developed. *Allerton* [1998] has pointed out that if the total slip on a thrust exceeds the displacements associated with vertical

axis rotation during thrusting, then all the boundaries of the rotating thrust sheet may be contractional.

#### 5.1.4. Implications of the Rotations

[50] The predominantly clockwise pattern of vertical axis rotations has two important implications. First, they demonstrate the existence of a significant component of strike-parallel shear during the contractional tectonic event. We can estimate this shear strain crudely if we treat the rotating blocks as being approximately circular (which is not far from the truth), and assume that they have rotated in response to tractions on their boundaries (implying that they are mechanically coupled one to another). The shear strain (gamma) is then equal to the spatially averaged rotation in radians. Excluding for the moment the small blocks that show very large rotations within the Crevillente fault zone, the average rotation is 0.66 rad. This indicates a strike-parallel displacement of 41 km across the 63 km width of the eastern Subbetic. It is possible to estimate the displacement within the Crevillente fault zone in a similar way. Figure 7 shows the locations of the kilometer-sized blocks that have experienced rotations of the order of 180° [*Allerton et al.*, 1993]. These are distributed over a zone ~10 km wide around the Crevillente fault. They are isolated, subcircular blocks surrounded by deformed Triassic marl and evaporites and hence can be approximated as rigid circular blocks rotating independently in a viscous matrix. In this case, the shear strain is equal to twice the block rotation in radians [*Lamb*, 1987]. Taking an average rotation of $\pi/2$ rad and assuming dextral shear, the strike-parallel displacement in the fault zone is 31 km. This gives a total of 72 km strike-parallel displacement for the Subbetic as a whole.

[51] Second, the implication of the vertical axis rotations is that the orientations of structures such as fold hinges and slip vectors cannot be taken at face value: depending on when they formed with respect to the timing of rotation, they may have been reoriented to a greater or lesser extent. To assess the extent of reorientation, we have constructed correlation plots relating fold hinges and slip vectors to vertical axis rotations (Figures 9b and 9c). This test is hindered by the fact that most of the paleomagnetic data were collected from regions of undeformed limestone, whereas most of the kinematic data come from regions of deformed Cretaceous and Tertiary marlstones which readily preserve calcite fiber lineations but which are not well suited for paleomagnetic work. A correlation plot of slip vectors against vertical axis rotations using the available data (13 sites) gives a slope of 0.71 ± 0.19 with an intercept at zero rotation of 306° ± 13° (Figure 9c).

[52] An alternative approach is to use our determination of the unrotated fold trend (029° ± 10°) from the more abundant data on the relationship between fold trends and vertical axis rotations and then to use the data on slip vectors and fold trends to determine the unrotated lineation trend. The intercept of the regression line for slip vectors against fold trends at a trend of 029° is 310° (Figure 9a), implying that lineations were formed with this trend prior to rotation. The uncertainty range on Figure 9a, allowing for summation of errors on the two regressions, is from 294° to 320°. The results from these two methods of determination are therefore within the uncertainties.

#### 5.1.5. Summary

[53] The eastern Subbetic has experienced a component of 139 ± 47 km of shortening toward 320°. The interrelationships among structural trends, fault slip vectors, and vertical axis rotations suggest that major folds and thrusts were initiated with a mean trend of 029° ± 10° and that the displacement direction during thrusting was 306° ± 13°. The amount of shortening in the transport direction calculated from this value is 153 km to 306°, and the component of motion parallel to strike (065°) is 74 ± 26 km. This compares well with the 72 km strike-parallel component of motion calculated directly from the vertical axis rotations (note that although the rotation data enter into both, these are independent methods of calculation). Shortening across the entire thrust belt in the eastern Betics, obtained by adding the estimates from the Fuensanta-Nerpio and Cazorla sections, is 191.5 ± 69 km to 317°, corrected to 212 ± 76 km to 306°.

### 5.2. Western and Central Subbetic

[54] The Central and Western Subbetic differ from the Eastern Subbetic in the following respects: (1) They front onto the Guadalquivir foreland basin, rather than onto the Prebetic thrust belt (Figure 1); facies equivalents of the Prebetic probably exist at depth beneath the Subbetic: they are locally exposed in the Jaén region [*García-Hernandez et al.*, 1980] and have been recovered from drill holes west of Ronda [*Flinch et al.*, 1996]. (2) The external Subbetic becomes progressively less coherent and recognizable as a discrete facies zone toward the west. (3) The facies in the median Subbetic become progressively deeper water, and may show a transition into the Cretaceous flysch domain west of Ronda [*Thurow and Kuhnt*, 1986]. (4) The proportion of chaotic rocks, dominated by Triassic evaporites, increases toward the west. (5) From Granada westward, the internal boundary of the Subbetic becomes a WNW directed forethrust (Figure 1), which emplaces various rocks of the Internal Zones over the internal Subbetic (commonly referred to in the west as the Penibetic). Sedimentary sequences ranging up to early Burdigalian (early Miocene) in age are present beneath the thrust [*González Donoso et al.*, 1987; *Martín-Algarra*, 1987], and it is overlain unconformably in several places by Tortonian (late Miocene) sediment, suggesting that the main phase of motion was early to middle Miocene in age [*Estévez et al.*, 1984; *Martín-Algarra*, 1987].

[55] In the westernmost part of the area, near Gibraltar, the major structures in the Internal Subbetic and Flysch units swing to a south trend, forming a major antitaxis within the Betic-Rif arc (Figure 1). The structural geometry in this area is locally complex, and exposure in the flysch is poor, hindering structural analysis. The south trend in the Gibraltar area is defined in part by large-scale folds that refold the thrusts and related smaller-scale structures. These folds are contractional structures and are likely to be related to underlying thrust culminations. They locally interfere

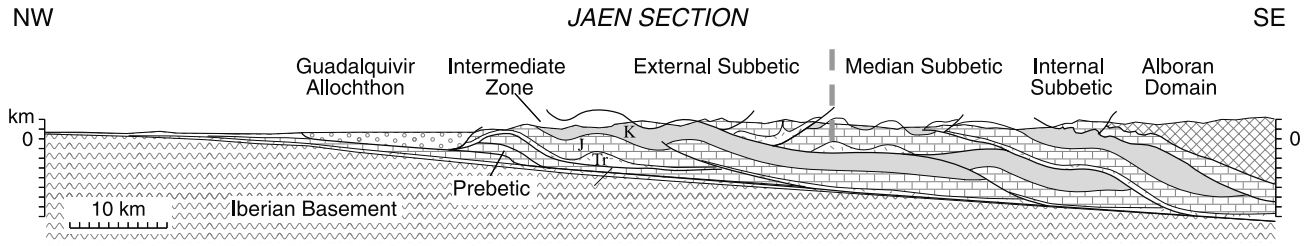


**Figure 10.** Jaén section (central Subbetic) (see Figure 1 for location). Modified after *Blankenship* [1992], *García-Hernandez et al.* [1980], and *Sanz de Galdeano et al.* [1993]. The boundary between the Median and External Subbetic in this section is a stratigraphic transition. Deep structure and depth to basement are based on seismic profiles. See color version of this figure at back of this issue.

with differently oriented older folds, producing interference structures, the most dramatic of which is the Las Cabras structure, west of Ronda (LC Figure 1). This is an E-W trending large-scale nearly isoclinal upright fold in the Median Subbetic that has been refolded about a N-S trend to produce a vertically plunging second-phase fold. The antitaxis therefore reflects the superposition of two differently oriented sets of structures. Our data suggest, however, that the older contractional structures in the internal Subbetic also swing into a more southerly trend, but less abruptly than the map pattern suggests. We present two balanced sections, across the Central and Western Subbetic, to illustrate the structure at depth and to provide a basis for estimates of shortening.

#### 5.2.1. Jaén Section

[56] The cross section (Figure 10, see Figure 1 for location) is based on the seismic data and interpretations presented by *Blankenship* [1992], modified after *García-Hernandez et al.* [1980] and *Sanz de Galdeano et al.* [1993]. *Blankenship* [1992] suggested that the Internal and External Subbetic domains form part of a single continuous thrust sheet of internal origin, now largely eroded away. This increased her estimates of shortening, and it requires a significant amount of material to have been eroded from above the present-day section. *Sanz de Galdeano et al.* [1993] disputed this interpretation, and we find their arguments convincing. The low maturity of median Subbetic sediments, indicated by vitrinite reflectance and pyrolysis data and the preservation of opal CT, suggests that there has not been more than ~1000 m of erosion from above the Median Subbetic [*Reicherter et al.*, 1994].

[57] The section trends toward 320°. The component of shortening within in the thrust wedge in this direction, based on line balancing the Jurassic carbonate section, is 147 km, plus a minimum of 19 km displacement on the IEZB, giving 166 km shortening over a present-day section length of 101 km. Using an area balance approach, this estimate implies an average stratigraphic thickness in the Prebetic and Subbetic (excluding the Internal Subbetic) of 2880 m. This estimate is consistent with the seismic sections and surface geology, although the original thickness of the Triassic section is very poorly constrained. The uncertainty is about ±300 m, giving an uncertainty on the shortening estimate of ±27 km. There is also some uncertainty about the origin and nature of the Guadalquivir allochthonous unit, which consists of chaotic material, predominantly of Triassic origin, known mainly from the subsurface in the frontal part of the thrust belt. This was traditionally thought to have been emplaced by gravity sliding or by sedimentary processes (e.g., as olistrostromes), implying zero shortening for this unit. *Blankenship* [1992] treats it as a thrust sheet lying in front of the Prebetic and neglects internal deformation, being impossible to estimate. This implies a shortening equal to the cross-sectional length of the unit (17.5 km). The cross section by *García-Hernandez et al.* [1980] implies that it originated at the base of the "intermediate unit" between the Prebetic and the External Subbetic. This does not change the shortening estimate. A more likely origin in paleogeographic terms, however, is that it comes from the Median Subbetic, which is characterized by a thick and evaporite-rich Triassic section. This interpretation requires 24.6 km shortening. Our estimate therefore includes 12.3 km of shortening, with ±12.3 km additional uncertainty. The depth to basement is constrained by the seismic profiles, with an uncertainty that increases to ±1 km at the internal end. This gives an additional uncertainty in the shortening estimate of ±18 km. The total uncertainty is therefore ±57 km.

[58] The original shortening direction in the central Subbetic is not well established, but it is likely to lie between our estimates for the eastern Subbetic (310°) and the western Subbetic (295°, see below). The orientation of the Tiscar transfer fault (310°) may indicate the approximate motion direction during the late Miocene. We have assumed a value of 300°. Hence the shortening estimate made along the line of section has to be corrected to the true shortening direction, giving 196 ± 67 km.

#### 5.2.2. Ronda Section

[59] In the western Subbetic the original shortening direction is well constrained at 295° [*Kirker and Platt*, 1998]. We have drawn the section (Figure 11) in this orientation from the Serrania de Ronda to the Bornos I well west of Ronda, where it links with the section published by *Flinch* [1996], drawn at 315°. The surface structure is after *Kirker and Platt* [1998] and *Bourgois* [1977]. The structure at depth is schematic, with the main boundaries projected from the southern part of Flinch's section. We have used the area balance technique to estimate the shortening over the combined section (from the IEZB to the thrust front). After correcting the estimates from the northern part of Flinch's

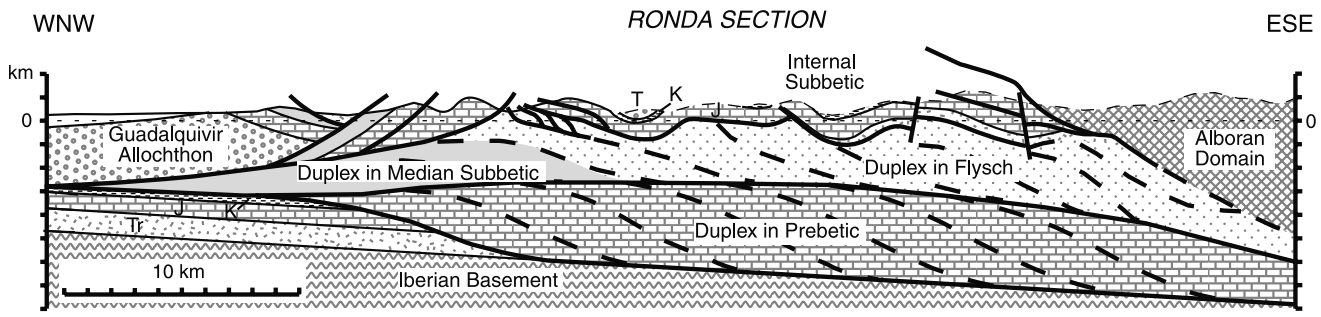


**Figure 11.** Ronda section (western Subbetic, see Figure 1 for location). Modified after *Flinch et al.* [1996] and *Kirker and Platt* [1998]. Only southeast part of the section is shown. Deep structure and depth to basement are constrained by drill hole data and seismic profiles. See color version of this figure at back of this issue.

section to the correct shortening direction, the shortening comes to 203 km in the Subbetic thrust wedge, plus 18 km displacement on the IEZB, over a section length of 113 km. We have assumed that the Guadalquivir allochthon is a thrust sheet, as it contains coherent layers of evaporites up to 200 m thick [*Flinch*, 1996]. The shortening in the wedge is made up of 118 km displacement of the Guadalquivir allochthon plus Median Subbetic plus flysch over the para-autochthonous sequence, 29 km displacement of Penibetic over Median Subbetic, 20 km shortening within the Subbetic and flysch in the area of Figure 10, 10 km shortening within the Guadalquivir allochthon (in Flinch's section), and 26 km shortening within the Prebetic duplex. The shortening estimates are based on assumed stratigraphic thicknesses, as follows: Prebetic 1890 m (from Flinch's section), Trias of Guadalquivir allochthon 2000 m, Median Subbetic 2700 m, Boyar corridor flysch zone 2400 m (from Bourgois' sections), Gibraltar flysch 2100 m (this assumes that the Tertiary flysch lies stratigraphically on a Mesozoic section showing a transition from Penibetic to Almarchal/Tangier unit stratigraphy). The assumed average stratigraphic thickness is 2100 m, with an uncertainty of ±400 m. This gives an uncertainty of ±34 km in the shortening estimate. The depth to basement is constrained by the seismic profiles, with an uncertainty that increases to ±1 km at the internal end. This gives an additional uncertainty in the shortening estimate of ±27 km and hence a total uncertainty of ±61 km.

### 5.2.3. Kinematic and Paleomagnetic Data

[60] Structural and kinematic data from the western Subbetic have been presented and analyzed in the light of the paleomagnetically determined vertical axis rotations by *Platzman* [1994], *Platt et al.* [1995], *Kirker and McClelland* [1996], and *Kirker and Platt* [1998] and are summarized here briefly.

[61] Slip vectors associated with the mappable thrusts vary considerably in orientation on a local scale, but when averaged over areas of a few square kilometers, the majority of the data have a remarkably consistent WNW trend from Granada right around the western Subbetic antitaxis to Gibraltar (Figure 2a). The structural trend, determined by the trend of major folds and thrust traces, swings through more than 60°, from 050° to 350°. This relationship is illustrated in Figure 10a, which shows the relationship between thrust slip vectors and structural trend. For this plot we have taken, where possible, the trends of folds that are clearly related to the thrusts, as these are not always parallel to the major folds that refold the thrusts. The overall swing in trend, however, is dominated by the effects of the late folds.

[62] Figure 12a suggests that the thrusting direction is largely independent of the overall swing in structural trend. There are two local exceptions that we are aware of. Local NNW directed thrusting west of Ronda (S Villalengua in Table 1 and Figure 12b) may be a result of a late clockwise rotation associated with an out-of-sequence thrust in the area [*Kirker and McClelland*, 1996]. SW directed lineations in a small region south of Gaucín (S Gaucin in Table 1 and Figure 12b) may be a result of a late anticlockwise rotation of ∼40° associated with a N-S trending sinistral fault [*Platt et al.*, 1995]. If these locations are omitted, the remaining slip vector data define a mean trend of 295° ± 8°.

[63] The independence of slip vectors from the structural trend in the western Betics is in marked contrast to the situation in the eastern Betics, described above. It suggests that the main phase of motion on the thrusts in the western Betics largely postdates creation of the arcuate structure and hence, by implication, that the arcuate structure is not a consequence of variations in the thrusting direction. Further discussion of this point requires us to take the pattern of vertical axis rotations into account.

[64] The main variation in structural trend around the western Subbetic antitaxis is largely independent of the amount of rotation: a change of trend of 90° from 080° to 350° occurs with only ∼35° poorly correlated variation in rotation (Figure 12b). The main exceptions to this picture are the area south of Gaucín, which may have experienced a late anticlockwise rotation as discussed above, and the Sierra Gorda (locations in Figure 1). The north trending structures in the Sierra Gorda clearly formed in that orientation and have not been subsequently rotated [*Platzman*, 1994]. The rocks involved in north trending structures near

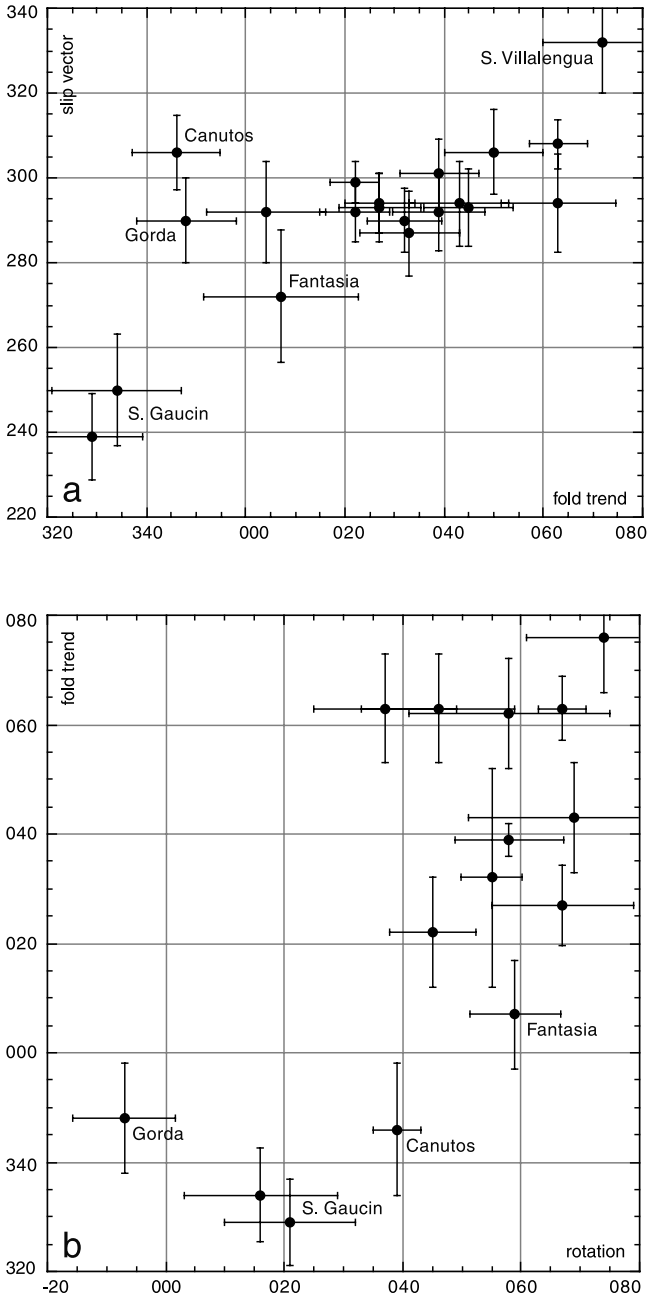


**Figure 12.** Correlation plots for western Subbetic. (a) Slip vectors against fold trends. (b) Fold trends against vertical axis rotations.

Gibraltar (locations Sierra Fantasia and Los Canutos in Figure 12b), however, appear to have been rotated by 40° or more, as much as the ENE trending structures around Ronda. *Platt et al.* [1995] used this relationship to infer that at least 40° of clockwise rotation has been imposed independently of the arcuate structure in the Gibraltar area and that formation of the antitaxis only involved ~35° of differential rotation.

[65] Further information on the timing and mechanism of the vertical axis rotations comes from consideration of the slip vector data. It is clear that the slip vectors have not experienced significant clockwise rotation: if that were the case, the original thrusting direction would have been away from, rather than toward, the Iberian margin. The main phase of rotation must therefore have preceded formation of the slip vectors. *Kirker and Platt* [1998] suggested that the rotations occurred at the start of thrusting, in response to oblique WNW directed convergence. Thrust sheets at the front of an oblique forward propagating system may rotate as they nucleate because they will propagate obliquely away from the thrust front and terminate in a tip line about which they will rotate [*Jolly and Sheriff*, 1992].

[66] We therefore suggest the following sequence of events to explain the pattern of structures, slip vectors, and vertical axis rotations in the western Subbetic (Figure 13).

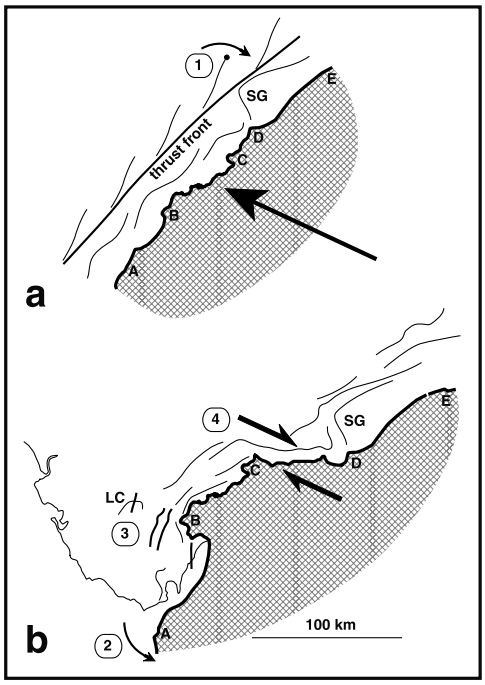


**Figure 13.** Formation of western Subbetic arc, modified after *Kirker and Platt* [1998]. (a) Initial stage of convergence, with NE trending margin converging at 295° with Subbetic basin. Newly formed thrusts propagate normal to convergence direction (1), and hence obliquely to thrust front. Thrust sheets rotate about thrust termination by up to 40° clockwise, to create sinuous trends in accretionary wedge. In the Sierra Gorda (SG), north trending thrusts controlled by preexisting normal faults do not rotate. (b) Part of extending Alboran domain rotates anticlockwise (2) to form Internal Rif. This creates corner in indentor at Gaucin (B). Continued WNW motion creates arcuate pattern of thrusts and folds around indenting corner (3): newly formed north trending folds (bold lines) locally refold older structures (e.g., Las Cabras, LC). Farther east, oblique convergence causes older structures to rotate further clockwise, tightening arc. Distributed shear in discrete shear corridors (4) results in particularly large rotations. A to E locate corresponding points in the two diagrams.

[67] 1. The margin of the Alborán Domain, where it impinged on the Subbetic basin, initially trended NE, with a relative motion direction toward 295°, oblique to the margin. Oblique convergence resulted in an initial rotation by up to 40° clockwise of thrust sheets as they nucleated (Figure 13a). The Sierra Gorda (SG in Figure 13), a N-S trending block of platform carbonates that was probably defined initially by Mesozoic normal faults, lay normal to the convergence direction and hence did not rotate. Oblique convergence at the thrust front, without partitioning of the strike-parallel component of motion onto a strike-slip fault at the rear of the thrust wedge, indicates a plastic bulk rheology for the wedge [*Platt*, 2000]. This is consistent with the fact that it comprises large sheets of massive carbonate rocks riding on Triassic evaporites.

[68] 2. During convergence, the geometry of the Alborán margin changed, and the segment now forming the northern Internal Rif rotated anticlockwise during extensional collapse of the Alborán Domain [*Platzman et al.*, 1993]. This produced a corner in the impinging margin, where the trend changed from NE to north (Figure 13b). Continued indentation of this corner into the previously deformed and rotated western Subbetic produced the presently observed arcuate pattern of fold and thrust trends, without only ~35° of differential rotation. North trending folds in the Gibraltar area formed during this stage, and refold earlier structures, at Las Cabras, for example (LC in Figure 13b).

[69] 3. Continued WNW convergence and displacement on the existing thrusts produced the observed pattern of WNW trending lineations.

[70] 4. Out-of-sequence thrusting in the S. Villalengua area, and sinistral strike-slip faulting south of Gaucín, produced local anomalies in the orientation pattern.

## 6. External Rif

[71] The External Rif represents the deformed sediments deposited on the northern passive margin of Africa. It is traditionally divided into the Prerif, Mesorif, and Intrarif domains, from more external (southerly) to internal (northerly) positions. Much of the Prerif is buried beneath the Neogene to Recent sediments of the foreland basin and the poorly understood "Prerif nappe": a chaotic mixture of Triassic evaporites and Mesozoic to early Miocene marly rocks. This has been interpreted as a complex of gravity slides and olistostromes [*Wildi*, 1983] or as an accretionary wedge [*Flinch*, 1996], emplaced in either case during the middle to late Miocene. Seismic profiles suggest that it has been affected by a combination of extensional and contractional deformation consistent with gravitationally driven flow [*Flinch*, 1996]. The Mesorif is a narrow and discontinuous zone of imbricated Mesozoic rocks, in platform carbonate facies up to the Lias, followed by Middle Jurassic siliciclastics and Cretaceous marls [*Wildi*, 1983]. The Intrarif is dominated by shales and fine-grained siliciclastic rocks of Middle Jurassic to Late Cretaceous age. The Internal Prerif, Mesorif, and Intrarif are overlain in places by Mesozoic to Tertiary thrust sheets of uncertain provenance. These include the Ouezzane nappe, the lower Rifian nappes, and the upper Rifian nappes, derived probably from the Mesorif or the external margin of the Intrarif. The Ouezzane nappe has been greatly disrupted, apparently by extensional flow in the underlying Prerif nappe [*Flinch*, 1996].

[72] The External Rif is overlain by the Flysch nappes, derived from a basin north of the African margin. These consist mainly of Early Cretaceous turbidites, deposited in a passive margin setting. They are divided on facies grounds into Mauretanian (more proximal) and Massylian (more distal) units. They are overlain by Late Cretaceous marls, followed by Oligocene micaceous flysch and late Oligocene to early Miocene quartz arenites, known as the Numidian flysch. The Tertiary sequences are grouped together as the Beni Ider nappe. The Oligocene micaceous flysch may be derived from the emerging collision zone in the Alborán Domain; otherwise, all these siliciclastic sequences are most plausibly derived from the African passive margin. Stratigraphically, the Massylian Flysch in particular is closely related to the Intrarif [*Didon et al.*, 1973], and structurally, the Flysch nappes form part of the external thrust belt, so they are treated here as part of the External Rif.

[73] The front of the External Rif is buried beneath the foreland basin and the Atlantic shelf and has been imaged seismically [*Flinch*, 1996]. The internal margin is defined by the thrust front of the Internal Rif (Alborán Domain), which is a continuation of the IEZB across the Strait of Gibraltar, and is for the most part a gently dipping thrust of probable Burdigalian age [*Wildi*, 1983; *Olivier*, 1981]. This thrust is cut and offset by the Jebha fault, a major sinistral strike-slip fault trending 070°. On the coast, at Jebha, the Jebha fault is vertical with an unambiguous sinistral slip sense, but farther west, around Cherafat (Figure 1), it loses its definition, and the IEZB is a gently dipping structure with south directed slip lineations [*Platzman et al.*, 1993]. The Jebha fault cannot be traced westward into the External Rif, and it probably transferred displacement from the extending Alborán Domain westward onto the IEZB [*Olivier*, 1981].

[74] Farther east, the External Rif is cut by another transfer fault, the Nekkor Fault. This is a major zone of sinistral strike-slip, trending 047°, with an estimated 50 km of displacement, which was active during the early Tortonian [*Leblanc and Olivier*, 1984]. It transfers displacement SW onto the Mesorif-Prerif boundary in the region of Dhar Souk. Like the Socovos fault in the Prebetics, it appears to be a thin-skinned transfer structure.

[75] The Mesorif, Intrarif, and Flysch nappes show evidence of a complex structural history. Primary thrusts are commonly folded on a large scale and even overturned, and they are cut by out-of-sequence thrusts, by strike-slip faults, and in places by normal faults. Cleavage and small-scale folds are widely developed, and in places, a second set of folds with an associated crenulation cleavage is developed [*Andrieux*, 1971]. In the Intrarif and adjacent Mesorif around Dhar Souk (Figure 1), *Andrieux* [1971] shows that early folds trending 240 to 270 are refolded by later structures trending more consistently WNW. The second phase folds affect sediments of Tortonian age. Farther east,

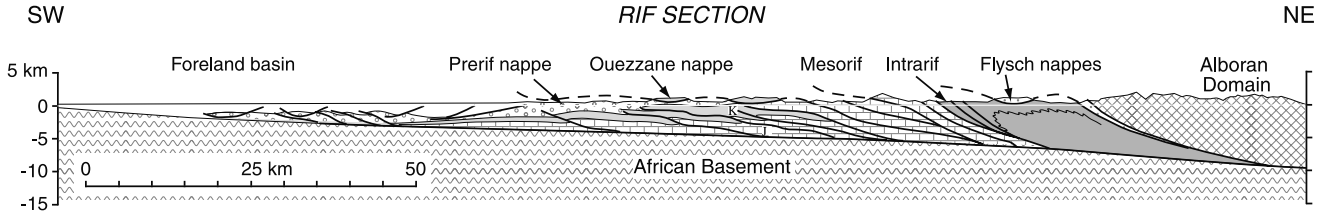


**Figure 14.** Section across the southwestern Rif (see Figure 1 for location). Modified after *Flinch* [1996] and *Wildi* [1983]. J, Jurassic; K, Cretaceous. Stratigraphy is greatly simplified for clarity: Triassic has been omitted from all units, and post-Jurassic rocks of the Mesorif are not distinguished. See color version of this figure at back of this issue.

in the Temsamane massif, *Frizon de Lamotte* [1987] shows that tight folds with associated slaty cleavage and a strong WSW trending stretching lineation were formed in late Serravallian to Early Tortonian time (about 11 Ma).

### 6.1. Rif Section

[76] The section across the Rif (Figure 14) was drawn across the southwestern section of the arc at 225°, roughly normal to the regional strike. The structure in the Prerif is based on the seismic interpretations of *Flinch* [1996], and in the more internal parts on the stratigraphic columns and sections of *Wildi* [1983] and our own observations. The component of shortening in the line of section is 205 km, made up of 19.4 km on the Prerif imbricates (from line balancing), 21.7 km displacement for the Ouezzane nappe (assuming that it has extended by a factor of 2 during flow in the underlying Prerif nappe), 52 ± 5 km in the Mesorif (area balanced assuming a stratigraphic thickness of 2400 ± 100 m to the top of the Jurassic), 42 km (30–64) in the Intrarif (area balanced assuming a stratigraphic thickness of 2100 ± 400 m for the Cretaceous and Tertiary section), 19.7 and 29.2 km displacement for the Massylian and Mauretanian flysch units, respectively, and 21.2 km displacement on the IEZB. The widespread occurrence of cleavage in the pelitic and calcareous rocks of the Mesorif and Intrarif suggests that up to 5 km has been eroded off these terrains: we have assumed that this was made up of the flysch units. Additional errors of ±15 km arise from the line balance and displacement estimates and ±10 km from the uncertainty of the depth to basement. A large uncertainty is added by the uncertain nature of the ''Prerif nappe,'' which we have treated as an essentially sedimentary deposit, implying no displacement. If it is in fact a thrust sheet, up to 70 km of additional displacement is implied. Internal shortening of the Prerif nappe is taken to be zero, as extensional structures appear to balance contractional structures in Flinch's sections. Minimum and maximum shortening estimates for the Rif section are therefore estimated at 161 and 325 km.

[77] We have insufficient kinematic data to constrain the true shortening direction along the line of section precisely. Our analysis below suggests that the original thrusting direction in the southern Rif was ~215°, but it is unlikely that the thrusting direction was constant around the arc, and along the section line it probably lies clockwise of this value. The Jebha fault, which lies close to the line of section, is a transfer fault trending 250°. A significant component of shortening across it is indicated by south directed thrust vectors along the trend (Figure 1), so the transport vector lies anticlockwise from 250°. An estimate of 235° ± 10° therefore seems reasonable. The shortening estimate corrected to this direction is 208 (163–330) km.

### 6.2. Structural and Paleomagnetic Data

[78] The aim of our research in the External Rif was to establish an integrated structural, kinematic, and paleomagnetic data set. To this end, we established new 35 study sites around the arc in Jurassic rocks of the Mesorif and adjacent units, which contain *ammonitico rosso* facies sequences that are potentially suitable for paleomagnetic work [*Favre et al.*, 1991]. We have also included in our analysis some kinematic data and one paleomagnetic site from the External Rif published by *Platzman et al.* [1993].

[79] In many locations the structure involves refolded thrusts, large-scale refolded folds, or refolded cleavage, suggesting polyphase deformation. The local structural trend is commonly defined by late folds with domal or irregular geometries suggestive of fold interference. Kinematic data were taken where possible from mappable thrust surfaces; they show consistently south trends, swinging from SW to SE around the arc (Figure 2a), and tend to be oriented at a high angle to the structural trend. This is brought out by the correlation plot (Figure 15a), which has a slope of 0.71.

[80] At each site we sampled *ammonitico rosso* facies limestones of either end Liassic or latest Jurassic age for paleomagnetic work. Nineteen sites yielded interpretable data, all from Early Jurassic sites; at the others we were unable to isolate unique components of magnetic remanence, and they had to be rejected. The data are summarized in Table 3. We only present data from the successful sites in this paper: information on the structural and paleomagnetic characteristics of the unsuccessful sites is presented in the auxillary data set.

[81] Our easternmost group of sites is in the Azrou Akchar window, which exposes Mesorif Jurassic beneath the predominantly Cretaceous Aknoul nappe (Figure 16). The window forms a thrust culmination over which the higher thrust sheets, including the overlying Aknoul nappe, are folded. The trend defined by these thrust-related folds is roughly NE, but the window has been modified by a normal fault on the north side and a N-S trending downwarp on the east. A good cleavage is developed in marly rocks through-

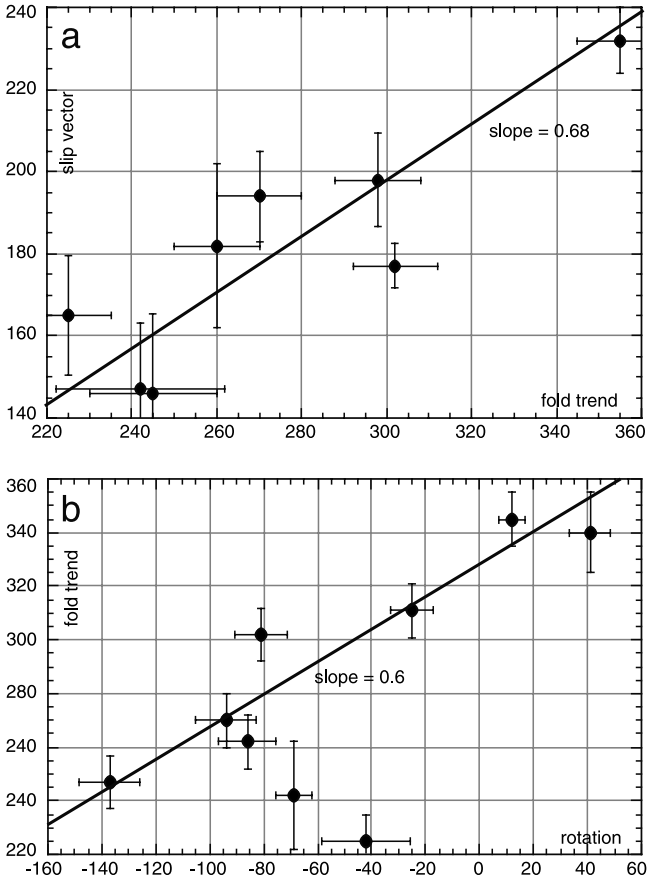


**Figure 15.** Correlation plots for the External Rif. (a) Slip vectors against fold trends. (b) Fold trends against vertical axis rotations.

out the massif, and the bedding/cleavage vergence is south to SE. Slip vectors on the major thrust faults trend fairly consistently SSE.

[82] Five paleomagnetic sites in the main Azrou Akchar limestone massif were studied. Anisotropy of magnetic susceptibility measurements indicate a weak (<6%) bedding-parallel fabric. Thermal demagnetization on most samples isolated a single stable component above ~200°C, which decayed to the origin by 650°C (e.g., sample R2-4a in Figure 17). These samples were analyzed by linear regression. In a few samples, there is evidence for more than one component, and the high-temperature component was not completely isolated by 615°C, where the intensity fell below the detection limit (e.g., sample R2-3a in Figure 17). The results show good intrasite correlation, but after tilt correction they are widely dispersed from site to site. The samples from all the sites cluster significantly better before tilt correction than after (Figure 17). The data both before and after tilt correction suggest large anticlockwise rotations (Table 3). We interpret these results as indicating a remagnetization event after the folding and faulting events that define the massif, followed by significant rotation. The most likely timing for remagnetization is during the Miocene contractional event. Relative to the Miocene reference direction for this location on the African plate (44°/000°) [*Besse and Courtillot*, 1991], the uncorrected data indicate 69° of anticlockwise rotation. The inclination is slightly shallow for the Miocene, which could result from a slight postmagnetization tilting. Because the remanences are postfolding, we lack a paleohorizontal reference frame to constrain this.

[83] A further five sites around a tight inclined fold in the Hajra Ali ridge SW of Azrou Akchar (Figure 16) were more difficult to interpret. Thermal demagnetization identified the presence of multiple components of remanence that could not be uniquely isolated by either thermal or alternating field treatment. Sample R32-11b in Figure 17 illustrates this mixed behavior, involving a lower temperature component with a shallow west plunge and a higher temperature component with a steeper north plunge. These mixed remanences fall on great circle trajectories, allowing the identification of prefolding and postfolding components (Figure 17). In some samples (e.g., R34-4b and R33-7b in Figure 17), a stable component could be identified at high temperature that was used as a fixed point for great circle analysis. The analysis identifies an intersection cluster before tilt correction directed NW and down, and a poorly

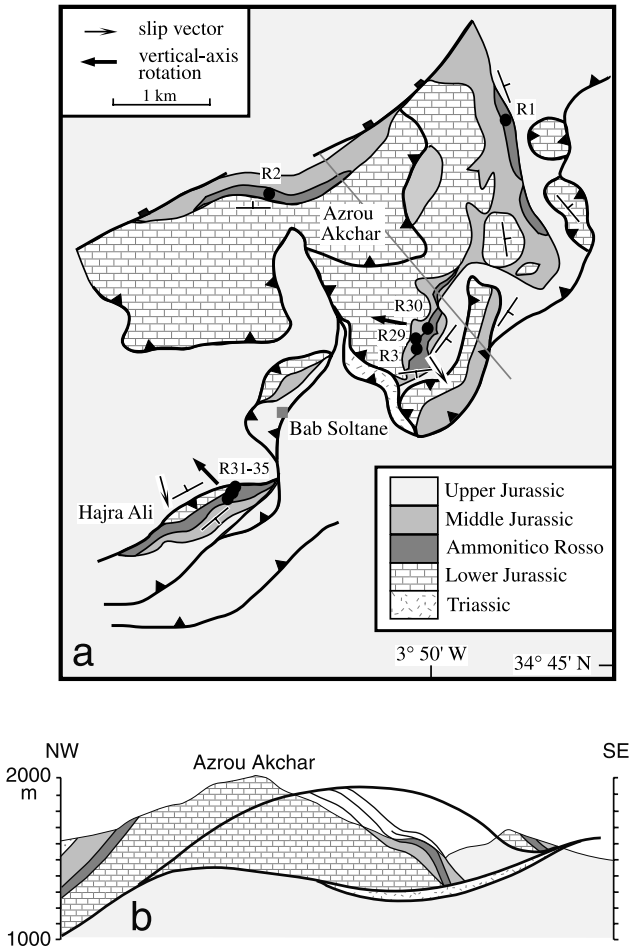


**Figure 16.** (a) Structural map and (b) section, Azrou Akchar area (AA in Figure 1).

defined cluster after tilt correction directed very steeply south and down. In view of the presence of cleavage and polyphase deformation in the area, these rocks may well have experienced remagnetization both before and after folding during the Miocene. The uncorrected intersection suggests 42° of postfolding anticlockwise rotation relative to the Miocene reference direction. The total rotation is likely to be much larger than this, but we cannot provide an unequivocal explanation of the steep inclination of the intersection cluster defined after tilt correction.

[84] We studied several groups of sites in the mountains north of Dhar Souk (Figure 18) in rocks of Mesorif facies but forming the stratigraphic and structural base of the Ketama group in the Intrarif [*Wildi*, 1983; *Asebriy et al.*, 1992]. The rocks in this area show strong cleavage and multiple lineations, which have been affected by late folding that controls the present-day structural trend [*Andrieux*, 1971]. At Chorfa el Olia in the Taffraount range, *ammonitico rosso* facies limestones have been thrown into a series of SW vergent overturned folds associated with thrusts. These folds have a strong axial plane cleavage and associated NW plunging intersection lineation. A stretching lineation is locally developed on the cleavage, with a mean plunge of 18°/038°. Slip vectors on thrust surfaces here and at El Merhour in the nearby Jebel Afress range trend due south. These structures have been refolded by small and large-scale folds trending E-W.

[85] We were only able to obtain useful paleomagnetic results from two of the 10 sites in these areas. At Sof Aouzzai, north of Dhar Souk, two sites fail a fold test; the result indicates 137° anticlockwise rotation after folding. At Tem bou Zid on the south flank of Jebel Tifelouest (site R6) we identified a single high-T remanence directed west and down (Table 3). We were not able to carry out a fold test, and within the uncertainty limits the inclination both before and after tilt correction is consistent with predicted Early Jurassic and Miocene inclinations. Given the presence of cleavage in the rocks and the widespread evidence for overprinting in the area, we have treated the remanence as a Miocene overprint. This implies a post-Miocene rotation of 84° anticlockwise. If the remanence is, in fact, primary, the total rotation is 105° anticlockwise.

[86] We studied four groups of sites in massive Lower Jurassic limestones of the Internal Prerif near Fes el Bali. No cleavage is developed in this area. At Derdaka, Aïn Lihamdi, and Beni Ouassal (sites R7-9 and R20), linear regression identified single high-temperature remanences: at Beni Ouassal, sites R9 and R20 pass a fold test, and at all three locations the inclinations after tilt correction (Table 3) are most consistent with the Early Jurassic reference direction (43°/337°) [*Besse and Courtillot*, 1991]. The data indicate vertical axis rotations varying from 12° clockwise to 94° anticlockwise relative to the Early Jurassic reference direction. Sites R17-19 at Mjaara showed evidence of overprinting, and great circle analysis identifies an intersection before tectonic correction directed NW and down. The inclination is relatively steep, consistent with a Miocene age. This suggests a posttilting rotation of 81° anticlockwise. The rotations at these locations correlate well with the variation in structural trend (Figure 19), suggesting that large differential vertical axis rotations have controlled the structure.

[87] Our most westerly site is in the north trending section of the Rif arc, and it was taken in Late Cretaceous limestones of the Massylian flysch unit [*Platzman et al.*, 1993]. This shows a clockwise rotation of 41° relative to the Early Cretaceous reference direction (38°/342°). This is consistent with the convergence direction of 235° we suggest for the northern Rif (see below), which has a slight dextral obliquity relative to the strike of this sector (340°).

### 6.3. Summary

[88] In spite of the difficulties in interpreting the paleomagnetic data, the results are surprisingly coherent. With the exception of the data from Azrou Akchar and Hajra Ali, all the data on fold trend and vertical axis rotation lie close to a regression line with a slope of 0.6 (Figure 15b). The rotation at Azrou Akchar, in common with several other sites, is a minimum value, as the remanence there is interpreted to be a postfolding overprint that may postdate part of the rotational history. Figure 15b suggests that the true value of the rotation there may be close to 180°. The regression line suggests that folds in the External Rif were initiated with a NW-SE trend (around 328°) and were subsequently rotated at about half the rate of material lines in the rocks. This interpretation requires that the fold hinges migrated with respect to the rock body, a situation characteristic of noncoaxial deformation (in this case, deformation with a large component of sinistral shear). The plot of slip vectors against fold rotation suggests that if the folds were initiated with a trend of 328°, the slip vectors would have been directed toward 215°. Note that the uncertainties on these estimates are large, but indeterminate, in view of the limitations of the paleomagnetic data. It is also likely that the transport direction changes significantly around the Rif arc, as we have shown is the case in the Betics. An initial thrusting direction of 215° may be approximately correct for the southern Rif, but as discussed above, we have assumed a value of 235° in the north.

## 7. Restoration of the Betic-Rif Arc

[89] We attempt to describe and constrain the kinematic evolution of the external Betic-Rif arc by restoring the boundary between the Alborán Domain and the thrust belt (the IEZB) to its configuration at the start of thrusting in early Miocene time, at approximately 19 Ma (Figure 20). We have done this by determining the transport vector for a series of sections across the arc using (1) structural and kinematic information, corrected where appropriate for the effects of vertical axis rotation, to determine the transport direction and (2) the shortening estimates from the balanced cross sections, corrected to the transport direction, for the displacement.

[90] Although the uncertainties on the shortening estimates are large, the constraints that they collectively place on the position and geometry of the IEZB are remarkably

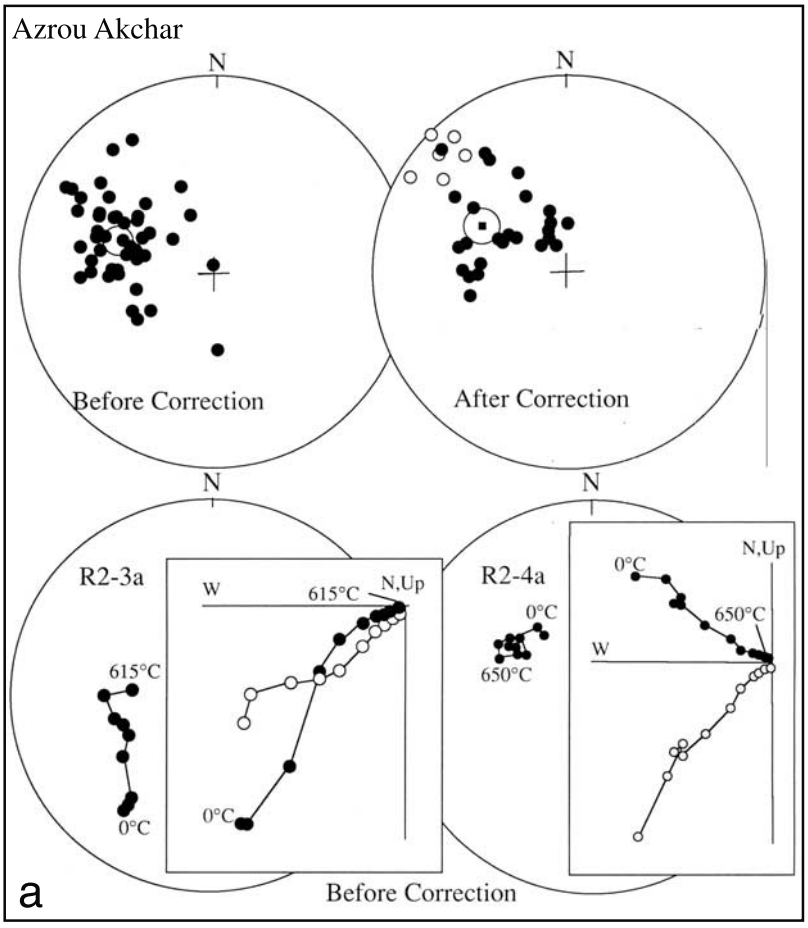
Azrou Akchar
N
Before Correction
After Correction
R2-3a
615°C
0°C
W
N,Up
R2-4a
650°C
a
Before Correction

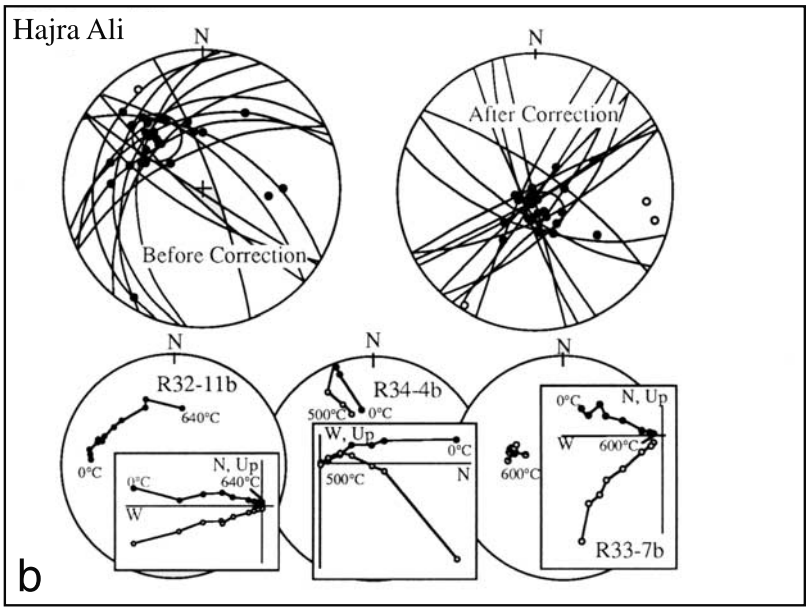
Hajra Ali
N
Before Correction
After Correction
R32-11b
640°C
0°C
N, Up
W
R34-4b
500°C
W, Up
R33-7b
600°C
b

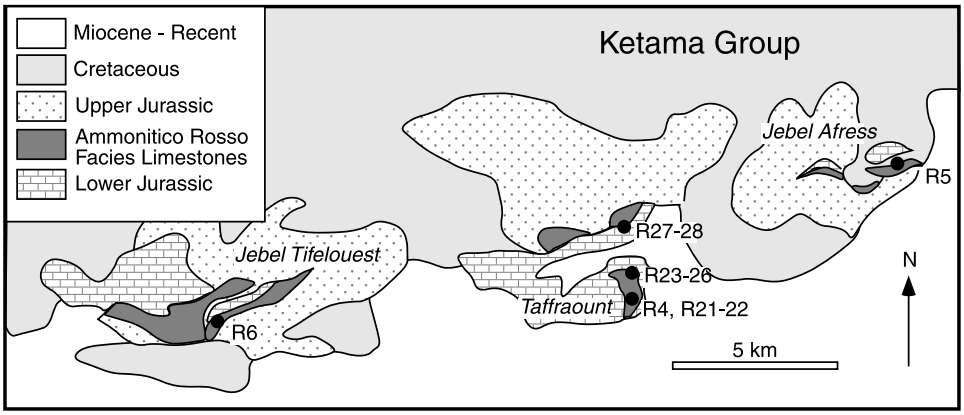


**Figure 18.** Outline geological map of area north of Dhar Souk (D in Figure 1). Study sites as follows: R4 and R21–22, Oued er Rhane; R5, El Merhour; R6, Tem bou Zid; R23–26, Chorfa el Olia; R27–28, Sof Aouzzai.

tight. The reconstruction shown is the only one possible that lies within the error limits of all the shortening estimates. It places the Alborán Domain during the early Miocene roughly 250 km ESE of its present position with respect to Iberia and 200 km ENE of its present position with respect to the African margin.

[91] The reconstructed average trend of the IEZB in the Betic sector is 040°, compared with the present trend of 065°. Note that this bulk rotation of 25° clockwise is constrained by the collective shortening estimate, and not by the paleomagnetic rotations. The much larger clockwise rotations observed in the Betics are a result of the motions of individual thrust sheets or stacks of thrust sheets on a scale of a few tens of kilometers during the contractional deformation. The reconstructed trend of the IEZB in the northern Rif is ~025°, close to its orientation in the Betic sector. This is constrained primarily by the paleomagnetic data for anticlockwise rotation of the Internal Rif [*Platzman et al.*, 1993; *Feinberg et al.*, 1996]. The clockwise rotations seen in the adjacent external zones (Gibraltar area and the northern External Rif) suggest that the present north trending sector of the arc was originally part of the dextrally oblique part of the converging margin. The IEZB in the southern sector of the Rif, on the other hand, appears to have been strongly rotated anticlockwise and substantially disrupted and extended by sinistral shear. The apex of the primary arc, separating the dextrally oblique from the sinistrally oblique part of the boundary, appears to have been near Cherafat, close to the present position of the Jebha fault zone.

[92] Overall, the IEZB has been substantially extended along its length during this evolution. This appears to be have been accomplished by displacement and shear along a number of fairly clearly identifiable transfer zones, indicated with broad shaded lines on Figure 20. These zones, with the displacements indicated by the reconstructed geometry of the IEZB, include the Socovos fault (22 km dextral), the Tiscar fault (50 km dextral), the Zegri shear zone (35 km dextral), the Malaga-Teba shear zone (60 km dextral), the Jebha fault (70 km sinistral), and the Nekkor fault (50 km minimum sinistral). These faults and shear zones have the effect of transferring displacement from the Alborán Domain, which was undergoing coeval extension, across the IEZB into the external thrust belt. The shear zones offset, rotate, and extend the IEZB, producing roughly E-W trending sectors of the boundary; they deflect the regional trend in the thrust belt, and they appear to be associated with regions of unusually large vertical axis rotation (Figure 2b). Within the Alborán Domain itself, these shear zones are associated with large rotations, as in the Malaga area [*Platzman et al.*, 2000], and are probably kinematically linked with the Miocene extensional basins in the Internal Betics. Note, however, that longitudinal extension of the external thrust belt was achieved by strike-slip faulting, not by normal faulting, as has been suggested for the Apennines [*Oldow et al.*, 1993]. This is consistent with the predictions of critical wedge theory applied to arcuate thrust belts [*Platt*, 2000].

[93] Strike-slip faulting has been invoked by numerous workers to explain aspects of the geometry of the Betic-Rif arc [e.g., *Paquet*, 1968; *Hermes*, 1978; *De Smet*, 1984; *Leblanc and Olivier*, 1984; *Sanz de Galdeano*, 1990]. These authors have generally identified faults trending between

**Figure 17.** (opposite) (a) Paleomagnetic data from sites R1–R3 and R29–R30, Azrou Akchar massif (see Figure 16). (top) High-temperature remanence directions from all samples, with mean and $\alpha 95$ confidence cones (equal angle projections, solid circles on lower hemisphere, open circles on upper hemisphere). Data cluster better before tilt correction than after. (bottom) Thermal demagnetization data from two representative samples. Solid circles on Zijderveld plots lie in the horizontal plane, and open circles lie in the vertical plane. (b) Paleomagnetic data from sites R31–35 on Hajra Ali ridge (see Figure 16). (top) Great circle analysis of remanence data from all sites. (bottom) Thermal demagnetization data from representative samples.

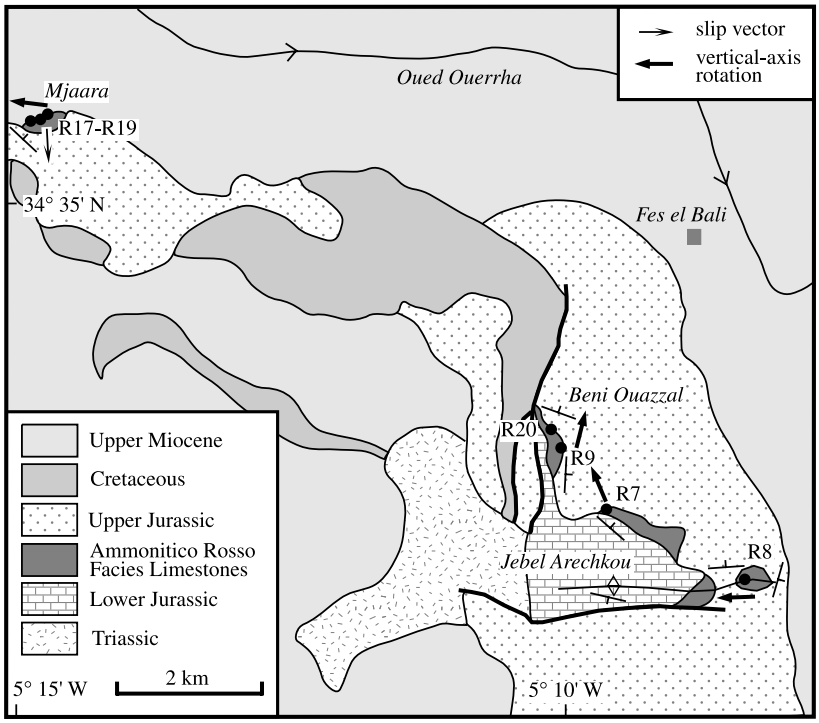


**Figure 19.** Structural map of the Fes el Bali area (FB in Figure 1).

070° and 090°, such as the Crevillente fault, as important dextral elements in the Betics. Few of these lineaments have demonstrable dextral displacements, however. The dextral faults and shear zones that we identify trend ESE, subparallel to the transport direction in the external thrust belt, and clearly offset or deform the IEZB and structures in the thrust belt.

### 7.1. Kinematics of Arc Formation

[94] Our analysis reveals that several separate processes contributed to the development of the arcuate geometry.

[95] 1. The initial cause was the westward component of motion of the Alborán Domain relative to the converging Iberian and African plates, as suggested by *Andrieux et al.* [1971]. The Alborán Domain terminated to the WSW, and in its initial stages the arc probably closed in this direction near Cherafat (Figure 20). At this stage the arc would have been nonrotational or primary, controlled by the geometry of the indenting Alborán Domain [*Hindle and Burkhard*, 1999; *Marshak*, 1988; *Macedo and Marshak*, 1999].

[96] 2. The present dramatic geometry of the arc is a result of the extensional collapse of the Alborán Domain during the Miocene. This modified the geometry of the western end of the arc, as the Internal Rif rotated anticlockwise, creating the second antitaxis in the Gibraltar area, and it produced additional components of displacement that were transferred into the external thrust belt along a series of transfer zones. These allowed the limbs of the arc to rotate and extend as it tightened. The Betic sector of the arc rotated clockwise by 25° during this process, and the southern Rif rotated anticlockwise by ~55° (Figure 20). This synorogenic bending is oroclinal in the sense that it changed the trend of preexisting structures. The evidence for this process comes primarily from displacement estimates based on section restoration.

[97] 3. Oblique convergence on the two limbs of the arc, dextral in the Betics and sinistral in the southern Rif, resulted in strongly noncoaxial deformation. This had three related effects (Figure 13). (1) Large rotations of individual thrust sheets resulted from the oblique propagation of thrusts away from the thrust front, followed by pinning and rotation as the thrust sheets peeled off. This process was particularly important in the western Subbetic [*Kirker and Platt*, 1998]. (2) Strike-parallel shear, concentrated in the rear of the thrust wedge [*Platt*, 2000], caused rotation of stacks of thrust sheets on the scale of a few tens of km; the amount of rotation is governed by the component of strike-parallel displacement and the width of the zone of distributed shear, and this process was probably responsible for much of the rotation seen in the eastern Subbetic. (3) Distributed shear in the orogen resulted in the rotation of folds as they amplified, the hinges migrating through the rock body and rotating at a slower rate than material lines in the rock. This process was particularly important in the Rif. These rotations, evidenced by paleomagnetic data, were substantially larger than the bulk rotations of the limbs of the arc, but they strongly modified the orientations of folds, thrust traces, and the structural indicators of fault slip directions.

### 7.2. Implications for the Evolution of the Alborán Domain

[98] Part of the motivation for this study was to understand better the geometrical and kinematic evolution of the Alborán Domain and its role in the formation of the external Betic-Rif arc. Our analysis reveals that in the early Miocene,

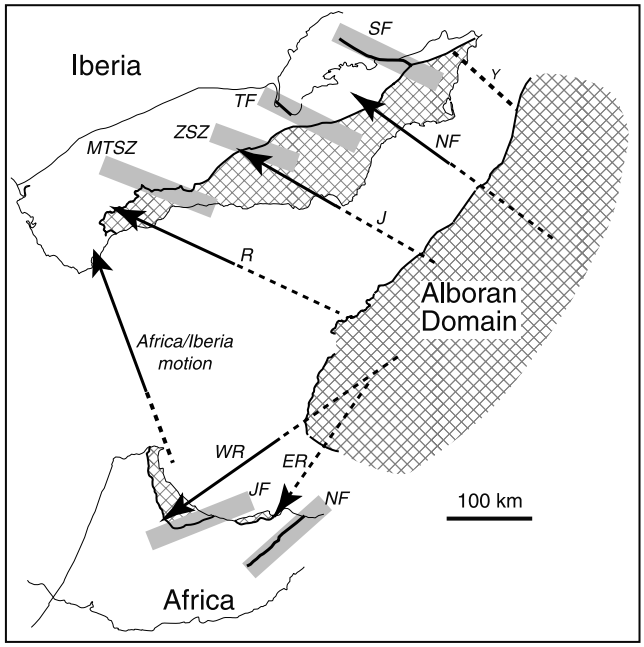


**Figure 20.** Palinspastic restoration of Betic-Rif arc. Reconstructed position and geometry of the Alborán Domain are constrained by displacement vectors determined from balanced cross sections as follows (from NE around the arc): Y, Yecla (estimate only); NF, Nerpio-Fuensanta and Cazorla lines; J, Jaén; R, Ronda; WR, Western Rif; ER, Eastern Rif (estimate only). Minimum displacements are shown with solid lines, total uncertainty is shown with dashed lines. Displacement along Nerpio-Fuensanta line is estimated from blind front of Alboran Domain beneath Internal Subbetic. Africa-Iberia motion since 19 Ma is after *Dewey et al.* [1989]. Transfer zones (in gray, from NE around the arc) are SF, Socovos fault; TF, Tiscar fault; ZSZ, Zegri shear zone; MTSZ, Malaga-Teba shear zone; JF, Jebha fault; NF, Nekkor fault.

early in the extensional collapse phase, it lay some 250 km westward of its present position (Figure 20) and had an orientation and a geometry consistent with it being the westernmost termination of the Alpine collisional orogen (see, for example, reconstructions by *Alvarez* [1976], *Dewey et al.* [1989], and many others). A purely kinematic analysis cannot reveal the cause of its subsequent westward motion, but it is worth noting that the Alborán Domain was only the western termination of a collapsing orogen that stretched across what is now the western Mediterranean. Collapse of this orogen led to the opening of the Balearic, Tyrrhenian, and Ligurian seas and may well have driven the westward motion of the Alborán Domain.

[99] As the Alborán Domain moved westward, the marine basins to its northwest, west, and southwest were progressively destroyed. These were occupied by the Mesozoic and Tertiary sediments of the Flysch nappes, the Subbetic, and the External Rif, now preserved in the external thrust belt. These basins must have been underlain mainly by stretched continental crust, judging by the abundance of Triassic evaporites in the thrust belt, but parts may have been oceanic. None of this basement is exposed at the surface. Part of it still underlies the emergent Internal Zones of the Betic Cordillera and Rif: the fact that these areas are now above sea level is due to the fact that they have been emplaced onto the Iberian and African margins [*Watts et al.*, 1993; *Carbonell et al.*, 1998]. There may still be a mass balance problem, however: an area of 136,000 km$^2$ of crust has disappeared (Figure 20), whereas the area that is presently underlain by this material is less than 40,000 km$^2$, where it makes up the lower 15–20 km of the crust. The implication is either that much of the crust that has disappeared was oceanic in character or that significant subduction of continental crust has occurred.

[100] Not only has the crust underlying these basins disappeared, so has the lithospheric mantle. The disappearance of 96,000 km$^2$ of lithosphere could reasonably be called subduction. The locus of this subduction was the IEZB, which has migrated westward with respect to both Africa and Iberia: in kinematic terms this is subduction rollback [*Lonergan and White*, 1997]. Whether rollback was driven by the subducting slab, however, depends on its buoyancy relative to the surrounding mantle. If the subducted lithosphere was continental in character, as suggested by the geological evidence, it is unlikely to have been able to drive rollback; if it was oceanic, as mass balance considerations may indicate, then the case is stronger.

[101] **Acknowledgments.** This work was supported by research grant GR3/7125 from the Natural Environment Research Council (NERC) in the U.K., by NERC studentships to C.M. and A.M., and a Commonwealth studentship to A.K. We are grateful to the Université Mohammed V of Rabat for logistical support during field work in Morocco and to Philippe Favre for his invaluable assistance in locating *ammonitico rosso* outcrops in the Rif. We thank Myrl Beck, Steve Marshak, David Evans, and Brian Wernicke for their careful work as reviewers and editors.

## References

Allerton, S., Vertical-axis rotation associated with folding and thrusting: An example from the eastern Subbetic zone of southern Spain, *Geology*, *22*, 1039–1042, 1994.

Allerton, S., Geometry and kinematics of vertical-axis rotations in thrust belts, *Tectonophysics*, *299*, 15–30, 1998.

Allerton, S., L. Lonergan, J. P. Platt, E. S. Platzman, and E. McClelland, Palaeomagnetic rotations in the eastern Betic Cordillera, southern Spain, *Earth Planet. Sci. Lett.*, *119*, 225–241, 1993.

Allerton, S., K. Reicherter, and J. P. Platt, A structural and palaeomagnetic study of a section through the eastern Subbetic, southern Spain, *J. Geol. Soc. London*, *151*, 659–668, 1994.

Alvarez, W., A former continuation of the Alps, *Geol. Soc. Am. Bull.*, *87*, 891–896, 1976.

Andrieux, J., *La Structure du Rif Central*, *Notes Mém Serv. Géol. Maroc*, *235*, 155 pp., Serv. Géol. du Maroc, Rabat, Morocco, 1971.

Andrieux, J., J. M. Fontboté, and M. Mattauer, Sur un modèle explicatif de l'arc de Gibraltar, *Earth Planet. Sci. Lett.*, *12*, 191–198, 1971.

Argand, E., La tectonique de l'Asie, in *13th International Geological Congress, Brussels 1924, Comptes Rendus*, *5*, 171–372, 1924.

Argles, T. W., J. P. Platt, and D. J. Waters, Attenuation and excision of a crustal section during extensional exhumation: The Carratraca Massif, Betic Cordillera, southern Spain, *J. Geol. Soc. London*, *156*, 149–162, 1999.

Asebriy, L., J. Bourgois, P. de Luca, and J. Butterlin, Importance d'une tectonique de distension pliocène dans le Rif central (Maroc): La nappe de Ketama existe-t-elle?, *J. Afr. Earth Sci.*, *15*, 49–57, 1992.

Ave-Lallemant, H. G., Displacement partitioning and arc-parallel extension in the Aleutian volcanic island arc, *Tectonophysics*, *256*, 279–293, 1996.

Azañon, J.-M., and A. Crespo-Blanc, Exhumation during a continental collision inferred from the tectonometamorphic evolution of the Alpujarride complex in the central Betics (Alborán Domain, SE Spain), *Tectonics*, *19*, 549–565, 2000.

Banda, E., J. Gallart, V. García-Dueñas, J. J. Dañobeita, and J. Makris, Lateral variation of the crust in the Iberian peninsula: New evidence from the Betic Cordillera, *Tectonophysics*, *221*, 53–66, 1993.

Banks, C. J., and J. Warburton, Mid-crustal detachment in the Betic system of southern Spain, *Tectonophysics*, *191*, 275–289, 1991.

Baranowski, J., J. Armbruster, N. Seeber, and P. Molnar, Focal depths and fault plane solutions of earthquakes and active tectonics of the Himalaya, *J. Geophys. Res.*, *89*, 6918–6928, 1984.

Beck, M., R. R. Burmester, R. E. Drake, and P. D. Riley, A tale of two continents: Some tectonic contrasts between the central Andes and the North American Cordillera, as illustrated by their paleomagnetic signatures, *Tectonics*, *13*, 215–224, 1994.

Bernoulli, D. and H. C. Jenkyns, Alpine, Mediterranean, and central Atlantic Mesozoic facies in relation to the early evolution of the Tethys, in *Modern and Ancient Geosynclinal Sedimentation*, edited by R. H. Dott and R. H. Shaver, *SEPM Spec. Publ*, *19*, 129–160, 1974.

Besse, J., and V. Courtillot, Revised and synthetic apparent polar wander paths of the African, Eurasian, North American and Indian plates, and true polar wander since 200 Ma, *J. Geophys. Res.*, *96*, 4029–4050, 1991.

Blanco, M. J., and W. Spakman, The *P*-wave velocity structure of the mantle below the Iberian Peninsula: Evidence for subducted lithosphere below southern Spain, *Tectonophysics*, *221*, 13–34, 1993.

Blankenship, C. L., Structure and palaeogeography of the External Betic Cordillera, southern Spain, *Mar. Pet. Geol.*, *9*, 256–264, 1992.

Bourgois, J., S'une étape géodynamique majeure dans la genèse de l'Arc de Gibraltar: L'hispanisation des flysch rifains au Miocène inférieur, *Bull. Soc. Géol. Fr.*, *19*, 1115–1119, 1977.

Bousquet, J. C., Quaternary strike-slip faults in southeastern Spain, *Tectonophysics*, *52*, 277–286, 1979.

Calvert, A., E. Sandvol, D. Seber, M. Barazangi, S. Roecker, T. Mourabit, F. Vidal, G. Alguacil, and N. Jabour, Geodynamic evolution of the lithosphere and upper mantle beneath the Alborán region of the western Mediterranean: Constraints from travel time tomography, *J. Geophys. Res.*, *105*, 10,871–10,898, 2000.

Carbonell, R., V. Sallarés, J. Pous, J. J. Dañobeita, P. Queralt, J. J. Ledo, and V. García-Dueñas, A multidisciplinary geophysical study in the Betic chain (southern Iberian Peninsula), *Tectonophysics*, *288*, 137–152, 1998.

Carey, S. W., The orocline concept in geotectonics, *Proc. R. Soc. Tasmania*, *89*, 255–288, 1955.

Comas, M. C., E. Puga, G. M. Bargossi, L. Morten, and P. L. Rossi, Paleogeography, sedimentation, and volcanism of the Central Subbetic Zone, Betic Cordilleras, Southeastern Spain, *Neues Jahrb. Geol. Paläontol. Monatsh.*, *7*, 385–404, 1986.

Comas, M. C., V. García-Dueñas, and M. J. Jurado, Neogene tectonic evolution of the Alborán Basin from MCS data, *GeoMar. Lett.*, *12*, 157–164, 1992.

Comas, M. C., J. P. Platt, J. I. Soto, and A. B. Watts, The Origin and Tectonic History of the Alborán Basin: Insights from Leg 161 Results, *Proc. Ocean Drill. Program Sci. Results*, *161*, 555–579, 1999.

Crespo-Blanc, A., Interference pattern of extensional fault systems: A case study of the Miocene rifting of the Alborán basement (north of Sierra Nevada, Betic Chain), *J. Struct. Geol.*, *17*, 1559–1570, 1995.

Davis, J. C., *Statistics and Data Analysis in Geology*, 2nd ed., 646 pp., John Wiley, New York, 1986.

DeMets, C., R. G. Gordon, D. F. Argus, and S. Stein, Current plate motions, *Geophys. J. Int.*, *101*, 425–478, 1990.

De Ruig, M. J., Fold trends and stress deviation in the Alicante fold belt, southeastern Spain, *Tectonophysics*, *184*, 393–403, 1990.

De Smet, M. E. M., Wrenching in the External Zone of the Betic Cordilleras, southern Spain, *Tectonophysics*, *107*, 57–79, 1984.

Dewey, J. F., M. L. Helman, E. Turco, D. W. H. Hutton, and S. D. Knott, Kinematics of the western Mediterranean, in *Alpine Tectonics*, edited by M. P. Coward, et al., *Geol. Soc. Spec. Publ.*, *45*, 265–284, 1989.

Didon, J., M. Durand-Delga, and J. Kornprobst, Homologies géologiques entre les deux rives du détroit de Gibraltar, *Bull. Soc. Géol. Fr.*, *15*, 77–105, 1973.

Empreza Nacional Adara de Investigaciones Mineras S.A. (ENADIMSA), Mapa geologico-minero de Andalucia, Junta de Andalucia, Sevilla, 1985.

Estévez, A., J. M. González-Donoso, D. Linares, A. Martin-Algarra, C. Sanz de Galdeano, and F. Serrano, El cabalgamiento finiserravallense del norte de Sierra Arana (Cordillera bética). Observaciones sobre la caracterización biostratigráfica del serravallense, *Mediterranea Ser. Geol.*, *3*, 151–173, 1984.

Favre, P., G. Stampfli, and W. Wildi, Jurassic sedimentary record and tectonic evolution of the northwestern corner of Africa, *Palaeogeogr. Palaeoclimatol. Palaeoecol.*, *87*, 53–73, 1991.

Feinberg, H., O. Saddiqi, and A. Michard, New constraints on the bending of the Gibraltar arc from palaeomagnetism of the Ronda peridotites (Betic Cordilleras, Spain), in *Palaeomagnetism and Tectonics of the Mediterranean Region*, edited by A. Morris and D. H. Tarling, *Geol. Soc. Spec. Publ.*, *105, 43–52, 1996.*

Fisher, R. A., Dispersion on a sphere, *Proc. R. Soc. London, Ser. A*, *217*, 295–305, 1953.

Flinch, J. F., Accretion and extensional collapse of the external western Rif (northern Morocco), in *Peri-Tethys Memoir 2: Structure and Prospects of Alpine Basins and Forelands*, edited by P. A. Ziegler and F. Horvath, *Mem. Mus. Natl. d'Hist. Nat.*, *70*, 61–85, 1996.

Flinch, J., A. W. Bally, and S. Wu, Emplacement of a passive margin evaporitic allochthon in the Betic Cordillera of Spain, *Geology*, *24*, 67–70, 1996.

Frizon de Lamotte, D., Un exemple de collage synmétamorphe: La déformation miocène des Temsamane (Rif externe, Maroc), *Bull. Soc. Géol. Fr.*, *3*, 337–344, 1987.

García-Hernandez, M., A. C. Lopez-Garrido, P. Rivas, C. Sanz de Galdeano, and J. A. Vera, Mesozoic palaeogeographic evolution of the external zones of the Betic Cordillera, *Geol. Mijnbouw*, *59*, 155–168, 1980.

Geel, T., and T. B. Roep, Oligocene to middle Miocene basin development in the Vélez Rubio Corridor—Espuña (Internal-External zone Boundary); eastern Betic Cordilleras, SE Spain, *Geol. Mijnbouw*, *77*, 39–61, 1999.

González Donoso, J. M., D. Linares, A. Martín-Algarra, and F. Serrano, El complejo tectosedimentario del Campo de Gibraltar. Datos sobre su edad y significado geológico, *Bol. R. Soc. Esp. Hist. Nat. Geol.*, *82*, 233–251, 1987.

Gray, M. B., and J. Stamatakos, New model for evolution of thrust belt curvature based on integrated structural and palaeomagnetic results from the Pennsylvania salient, *Geology*, *25*, 1067–1070, 1997.

Grimison, N. L., and W. P. Chen, The Azores-Gibraltar plate boundary: Focal mechanisms, depths of earthquakes, and their tectonic implications, *J. Geophys. Res.*, *91*, 2029–2047, 1986.

Grubbs, K. L., and R. Van der Voo, Structural deformation of the Idaho-Wyoming overthrust belt (U.S.A.) as determined by Triassic paleomagnetism, *Tectonophysics*, *33*, 321–326, 1976.

Guezou, J. C., D. Frizon de Lamotte, M. Coulon, and J.-L. Morel, Structure and kinematics of the Prebetic nappe complex (southern Spain): Definition of a "Betic Floor Thrust" and implications in the Betic-Rif orocline, *Ann. Tectonicae*, *5*, 32–48, 1991.

Hermes, J. J., The stratigraphy of the Subbetic and southern Prebetic of the Velez Rubio - Caravaca area and its bearing on transcurrent faulting in the Betic Cordilleras of southern Spain, *Verh. K. Ned. Akad. Wet.*, *81*, 1–54, 1978.

Hindle, D., and M. Burkhard, Strain, displacement and rotation associated with the formation of curvature in folds belts; the example of the Jura arc, *J. Struct. Geol.*, *21*, 1089–1102, 1999.

Hossack, J. R., The use of balanced cross-sections in the calculation of orogenic contraction: A review, *J. Geol. Soc. London*, *136*, 705–711, 1979.

Isacks, B. L., Uplift of the central Andean Plateau and bending of the Bolivian Orocline, *J. Geophys. Res.*, *93*, 3211–3231, 1988.

Jabaloy, A., J. Galindo-Zaldívar, and F. González-Lodeiro, The Alpujarride-Nevado-Filabride extensional shear zone, Betic Cordillera, SE Spain, *J. Struct. Geol.*, *15*, 555–570, 1993.

Jolly, A. D., and S. D. Sheriff, Palaeomagnetic study of thrust sheet motion along the Rocky Mountain front in Montana, *Geol. Soc. Am. Bull.*, *104*, 779–785, 1992.

Kirker, A. and E. McClelland, Application of net tectonic rotations and inclination analysis to a high-resolution palaeomagnetic study in the Betic Cordillera, in *Palaeomagnetism and Tectonics of the Mediterranean Region*, edited by A. Morris and D. H. Tarling, *Geol. Soc. Spec. Publ.*, *105*, 19–32, 1996.

Kirker, A. I., and J. P. Platt, Unidirectional slip vectors in the western Betic Cordillera: Implications for the formation of the Gibraltar arc, *J. Geol. Soc. London*, *155*, 193–208, 1998.

Lamb, S., A model for tectonic rotations about a vertical axis, *Earth Planet. Sci. Lett.*, *84*, 75–86, 1987.

Leblanc, D., and P. Olivier, Role of strike-slip faults in the Betic-Rifian Orogeny, *Tectonophysics*, *101*, 345–355, 1984.

Lonergan, L., and N. White, Origin of the Betic-Rif mountain belt, *Tectonics*, *16*, 504–522, 1997.

Lonergan, L., J. P. Platt, and L. Gallagher, The Internal-External Zone Boundary in the eastern Betic Cordillera, SE Spain, *J. Struct. Geol.*, *16*, 175–188, 1994.

Macedo, J., and S. Marshak, Controls on the geometry of fold-thrust belt salients, *Geol. Soc. Am. Bull.*, *111*, 1808–1822, 1999.

MacFadden, B. J., F. Anaya, and C. C. Swisher, Neogene paleomagnetism and oroclinal bending of the central Andes of Bolivia, *J. Geophys. Res.*, *100*, 8153–8167, 1995.

Malinverno, A., and B. Ryan, Extension in the Tyrrhenian Sea and shortening in the Apennines as a result of arc migration driven by sinking of the lithospere, *Tectonics*, *5*, 227–245, 1986.

Mandeville, C. R. M., A structural study of an Arcuate Thrust Belt, Prebetic Zone, southern Spain, Ph.D. thesis, Univ. of Oxford, Oxford, U.K., 1993.

Marshak, S., Kinematics of orocline and arc formation in thin-skinned orogens, *Tectonics*, *7*, 73–86, 1988.

Marshak, S., and T. Flöttman, Structure and origin of the Fleurieu and Nackara Arcs in the Adelaide fold-thrust belt, South Australia: Salient and recess development in the Delamerian Orogen, *J. Struct. Geol.*, *18*, 891–908, 1996.

Marshak, S. M., and J. Tabor, Structure of the Kingston orocline in the Appalachian fold-thrust belt, New York, *Geol. Soc. Am. Bull.*, *101*, 683–701, 1989.

Martín-Algarra, A., Evolucion geologica Alpina del contacto entre las zonas Internas y las zonas Externas de la Cordillera Betica, Ph.D. thesis, Univ. of Granada, Granada, Spain, 1987.

Mayfield, A., Palaeomagnetic and kinematic constraints on deformation during oblique convergence, Betic Cordillera, southern Spain, Ph.D. thesis, Univ. of London, London, U.K., 1999.

McCaffrey, R., Global variability in subduction thrust zone-forearc systems, *Pure Appl. Geophys.*, *142*, 173–224, 1994.

Molnar, P. M., and H. Lyon-Caen, Fault plane solutions of earthquakes and active tectonics of the Tibetan Plateau and its margins, *Geophys. J. Int.*, *99*, 123–153, 1989.

Morel, J. L., and M. Meghraoui, Goringe-Alboran-Tell tectonic zone: A transpression system along the Africa-Eurasia plate boundary, *Geology*, *24*, 755–758, 1996.

Oldow, J. S., B. d'Argenio, L. Ferranti, G. Pappone, E. Marsella, and M. Sacchi, Large-scale longitudinal extension in the southern Apennines contractional belt, Italy, *Geology*, *21*, 1123–1126, 1993.

Olivier, P., L'accident de Jebha-Chrafate (Rif, Maroc), *Rev. Géol. Dyn. Géogr. Phys.*, *23*, 27–106, 1981.

Osete, M. L., R. Freeman, and R. Vegas, Preliminary palaeomagnetic results from the Subbetic Zone, (Betic Cordillera, southern Spain): Kinematic and structural implications, *Phys. Earth Planet. Inter.*, *52*, 283–300, 1989.

Paquet, J., *Étude Geologique de l'Ouest de la Province de Murcia*, *Mém. Soc. Géol. Fr.*, *48*, 270 pp., 1968.

Petit, J. P., Criteria for sense of movement on fault surfaces in brittle rocks, *J. Struct. Geol.*, *9*, 597–608, 1987.

Platt, J. P., Calibrating the bulk rheology of active obliquely convergent thrust and accretionary wedges from surface profiles and velocity distributions, *Tectonics*, *19*, 529–548, 2000.

Platt, J. P., and R. L. M. Vissers, Extensional collapse of thickened continental lithosphere: A working hypothesis for the Alborán Sea and the Gibraltar arc, *Geology*, *17*, 540–543, 1989.

Platt, J. P., and M. J. Whitehouse, Early Miocene high-temperature metamorphism and rapid exhumation in the Betic Cordillera (Spain): Evidence from U-Pb zircon ages, *Earth Planet. Sci. Lett.*, *171*, 591–605, 1999.

Platt, J. P., S. Allerton, A. Kirker, and E. S. Platzman, Origin of the western Subbetic arc, southern Spain: Palaeomagnetic and structural evidence, *J. Struct. Geol.*, *17*, 765–775, 1995.

Platt, J. P., J.-I. Soto, M. J. Whitehouse, A. J. Hurford, and S. P. Kelley, Thermal evolution, rate of exhumation, and tectonic significance of metamorphic rocks from the floor of the Alborán extensional basin, western Mediterranean, *Tectonics*, *17*, 671–689, 1998.

Platzman, E. S., Paleomagnetic rotations and the kinematics of the Gibraltar arc, *Geology*, *20*, 311–314, 1992.

Platzman, E. S., East-west thrusting and anomalous magnetic declinations in the Sierra Gorda, Betic Cordillera, southern Spain, *J. Struct. Geol.*, *16*, 11–20, 1994.

Platzman, E., and W. Lowrie, Palaeomagnetic evidence for rotation of the Iberian Peninsula and the external Betic Cordillera, southern Spain, *Earth Planet. Sci. Lett.*, *108*, 45–60, 1992.

Platzman, E. S., J. P. Platt, and P. Olivier, Palaeomagnetic rotations and fault kinematics in the Rif arc of Morocco, *J. Geol. Soc. London*, *150*, 707–718, 1993.

Platzman, E., J. P. Platt, and S. P. Kelley, Large clockwise rotations in an extensional allochthon, Alborán Domain (southern Spain), *J. Geol. Soc. London*, *157*, 1187–1197, 2000.

Puga, E., J. M. Nieto, A. Diaz de Federico, J. L. Bodinier, and L. Morten, Petrology and metamorphic evolution of ultramafic rocks and dolerite dykes of the Betic Ophiolite Association (Mulhacen Complex, SE Spain): Evidence of eo-Alpine subduction following an ocean-floor metasomatic process, *Lithos*, *49*, 23–56, 1999.

Reicherter, K., T. Pletsch, W. Kuhnt, J. Manthey, G. Homeier, J. Wiedmann, and J. Thurow, Mid-Cretaceous paleogeography and paleoceanography of the Betic Seaway (Betic Cordillera, Spain), *Palaeogeogr. Palaeoclimatol. Palaeoecol.*, *107*, 1–33, 1994.

Rey, J., Extensional Jurassic tectonism of the eastern Subbetic section (southern Spain), *Geol. Mag.*, *135*, 685–697, 1998.

Roest, W. R., and S. P. Srivastava, Kinematics of the plate boundaries between Eurasia, Iberia and Africa in the North Atlantic from the Late Cretaceous to the present, *Geology*, *19*, 613–616, 1992.

Royden, L. H., The tectonic expression of slab pull at continental convergent boundaries, *Tectonics*, *12*, 303–325, 1993.

Sanz de Galdeano, C., Geologic evolution of the Betic Cordilleras in the western Mediterranean, Miocene to present, *Tectonophysics*, *172*, 107–119, 1990.

Sanz de Galdeano, C., The E-W segments of the contact between the External and Internal Zones of the Betic and Rif Cordilleras and the E-W corridors of the Internal Zone (a combined explanation), *Estud. Geol.*, *52*, 123–136, 1996.

Sanz de Galdeano, C., A. Martin-Algarra, J. A. Vera, and P. Rivas, Comments on 'Structure and palaeogeography of the External Betic Cordillera, southern Spain' by C. L. Blankenship, *Mar. Pet. Geol.*, *10*, 518–521, 1993.

Sartori, R., L. Torelli, N. Zitellini, D. Peis, and E. Lodolo, Eastern segment of the Azores-Gibraltar line (central-eastern Atlantic): An oceanic plate boundary with diffuse compressional deformation, *Geology*, *22*, 555–558, 1994.

Schmid, S. M., and E. Kissling, The arc of the western Alps in the light of geophysical data on deep crustal structure, *Tectonics*, *19*, 62–85, 2000.

Seber, D., M. Barazangi, A. Ibenbrahim, and A. Demnati, Geophysical evidence for lithospheric delamination beneath the Alborán Sea and Rif-Betic mountains, *Nature*, *379*, 785–791, 1996.

Soto, J. I., and J. P. Platt, Petrological and structural evolution of high-grade metamorphic rocks from the floor of the Alborán Sea basin, western Mediterranean, *J. Petrol.*, *40*, 21–60, 1999.

Thurow, J. and W. Kuhnt, Mid Cretaceous of the Gibraltar arc area, in *North Atlantic Palaeoceanography*, edited by C. P. Summerhayes and N. J. Shackleton, *Spec. Publ. Geol. Soc.*, *21*, 423–445, 1986.

Torné, M., M. Fernandez, M. C. Comas, and J. I. Soto, Lithospheric structure beneath the Alborán Sea basin: Results from three-dimensional gravity modeling and tectonic relevance, *J. Geophys. Res.*, *105*, 3209–3228, 2000.

Vera, J. A., Las zonas externas, in *Geología de España (Libro Jubilar J. M. Rios)*, vol. 2, pp. 218–250, Inst. Geol. y Minero de Esp., Madrid, 1983.

Villalaín, J. J., M. L. Osete, R. Vegas, V. García-Dueñas, and F. Heller, Widespread Neogene remagnetization in Jurassic limestones of the South-Iberian palaeomargin (western Betics, Gibraltar Arc), *Phys. Earth Planet. Inter.*, *85*, 15–33, 1994.

Vissers, R. L. M., J. P. Platt, and D. van der Wal, Late orogenic extension of the Betic Cordillera and the Alborán Domain: A lithospheric view, *Tectonics*, *4*, 786–803, 1995.

Watts, A. B., J. P. Platt, and P. Buhl, Tectonic evolution of the Alborán Sea basin, *Basin Res.*, *5*, 153–177, 1993.

Weil, A. B., R. Van der Voo, B. A. van der Pluijm, and J. M. Parés, The formation of an orocline by multiphase deformation: A paleomagnetic investigation of the Cantabria-Asturias Arc, northern Spain, *J. Struct. Geol.*, *22*, 735–756, 2000.

Westphal, M., M. L. Bazhenov, J. P. Lauer, D. M. Pechersky, and J. C. Sibuet, Palaeomagnetic implications on the evolution of the Tethys belt from the Atlantic ocean to the Pamirs since the Triassic, *Tectonophysics*, *123*, 37–82, 1986.

Wildi, W., La chaine tello-rifaine (Algérie, Maroc, Tunisie): Structure, stratigraphie et évolution du Trias au Miocène, *Rev. Géol. Dyn. Géogr. Phys.*, *24*, 201–297, 1983.

S. Allerton, A. Kirker, and C. Mandeville, Department of Earth Sciences, University of Oxford, Parks Road, Oxford OX1 3PR, UK.

A. Mayfield, J. P. Platt, and E. S. Platzman, Department of Earth Sciences, University College London, Gower Street, London WC1E 6BT, UK. (John.Platt@ucl.ac.uk)

A. Rimi, Institut Scientifique, Université Mohammed V, B.P. 703, Rabat, Morocco.


**Figure 1.** Tectonic map of Betic-Rif arc, after *Empreza Nacional Adara de Investigaciones Mineras S.A.* (ENADIMSA) [1985] and *Wildi* [1983]. External thrust belt comprises Prebetic and Subbetic Zones in Spain; Prerif, Mesorif, and Intrarif zones in Morocco; and Flysch nappes, which straddle the Straits of Gibraltar. Alborán Domain comprises Betic and Rif Internal Zones, together with floor of the Alborán Sea. A, Alicante; C, Cherafat; D, Dhar Souk; G, Granada; Gu, Gaucín; J, Jaén; LC, Las Cabras; R, Ronda; SG, Sierra Gorda; T, Temsamane massif. Restored sections indicated, from NE around arc, are Y, Yecla; E, Elche; C, Cazorla (Figure 5); NF, Nerpio-Fuensanta (Figure 8); J, Jaén (Figure 10); R, Ronda (Figure 11); and WR, Western Rif (Figure 14). Locations of Figures 2 and 3 and maps of Azrou Akchar (AA, Figure 16), Dhar Souk (D, Figure 18), Fes el Bali (FB, Figure 19), and Sidi Redouane (SR, Figure A of auxillary data) are shown. Inset shows position of Betic-Rif arc in context of Mediterranean Alpine chains.

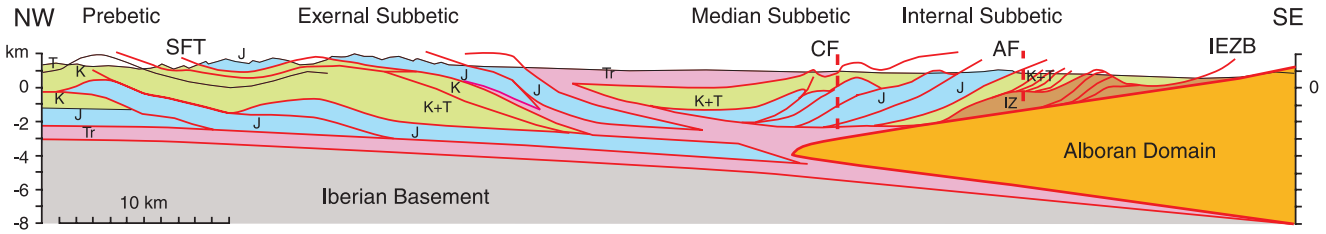


**Figure 8.** Nerpio-Fuensanta section (eastern Subbetic, see Figures 1 and 7 for location). The Crevillente and Almirez faults produce displacements out of plane of section. Structure at depth is constrained by seismic profiles [*Banks and Warburton*, 1991]; depth to basement is constrained by gravity modeling [*Mandeville*, 1993].

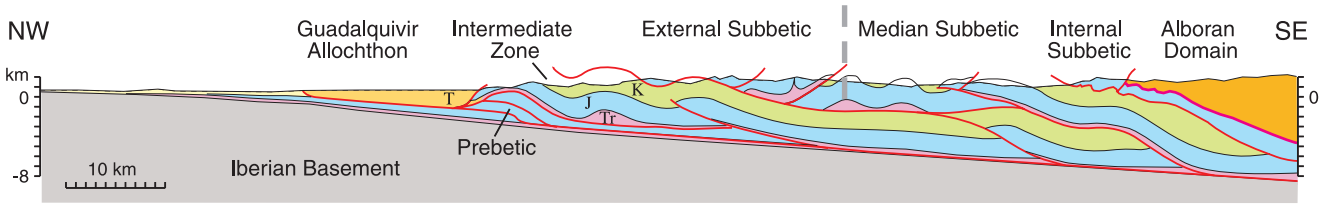


**Figure 10.** Jaén section (central Subbetic) (see Figure 1 for location). Modified after *Blankenship* [1992], *García-Hernandez et al.* [1980], and *Sanz de Galdeano et al.* [1993]. The boundary between the Median and External Subbetic in this section is a stratigraphic transition. Deep structure and depth to basement are based on seismic profiles.

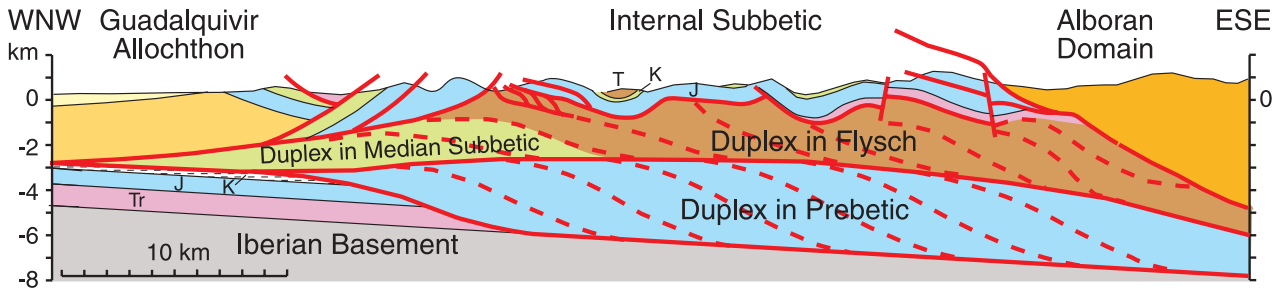


**Figure 11.** Ronda section (western Subbetic, see Figure 1 for location). Modified after *Flinch et al.* [1996] and *Kirker and Platt* [1998]. Only southeast part of the section is shown. Deep structure and depth to basement are constrained by drill hole data and seismic profiles.

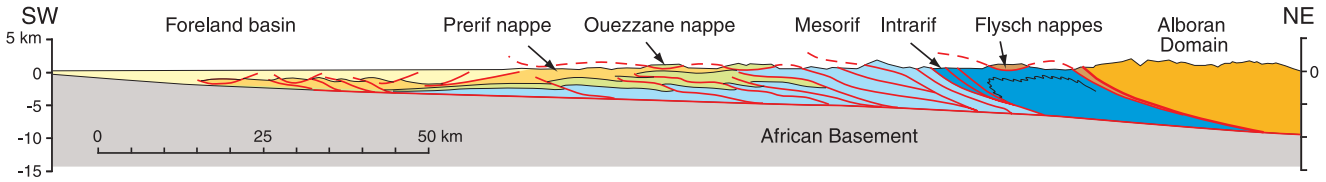


**Figure 14.** Section across the southwestern Rif (see Figure 1 for location). Modified after *Flinch* [1996] and *Wildi* [1983]. J, Jurassic; K, Cretaceous. Stratigraphy is greatly simplified for clarity: Triassic has been omitted from all units, and post-Jurassic rocks of the Mesorif are not distinguished.